MEASUREMENT OF THE VISCOELASTIC AND RELATED MASS-PHYSICAL PROPERTIES OF SOME CONTINENTAL TERRACE SEDIMENTS

by

George Edward Bieda

LIBRARY
NAVAL POSTGRADUATE SCHOOL
MONTEREY, CALIF. 93940

United States
Naval Postgraduate School

THESIS

MEASUREMENT OF THE VISCOELASTIC
AND RELATED MASS-PHYSICAL PROPERTIES
OF SOME CONTINENTAL TERRACE SEDIMENTS

by

George Edward Bieda

June 1970

This document has been approved for public release and sale; its distribution is unlimited.

Measurement of the Viscoelastic and Related Mass-Physical Properties of Some Continental Terrace Sediments

by

George Edward Bieda
Lieutenant Junior Grade, United States Navy
B.S., United States Naval Academy, 1969

Submitted in partial fulfillment of the
requirements for the degree of

MASTER OF SCIENCE IN OCEANOGRAPHY

from the

NAVAL POSTGRADUATE SCHOOL
June 1970

c.1

ABSTRACT

The complex rigidity of 20 samples of continental terrace clayey-silt sediments has been measured in the laboratory using a viscoelastometer in the frequency range from 4 to 38 kHz. The method involves measuring the effects on torsional waves propagating in a rod due to shear loading of the side walls of the rod when it is imbedded in the sediment. Values of the real component of rigidity range from 6.5×10^5 to 2.6×10^7 dynes/cm^2. Values of the imaginary component of rigidity fall between 2.9×10^5 and 8.2×10^6 dynes/cm^2. No clear-cut dependence of rigidity upon frequency is observed. Both real and imaginary components of rigidity are analyzed by plotting the data as a function of various other mass-physical properties, including: density, porosity, compressional sound speed, sand-silt-clay percentages, montmorillonite, chlorite, illite percentages, vane shear strength, Poisson's ratio, and the product of density and sound speed squared. These analyses indicate that both real and imaginary components of rigidity exhibit trends with some of the mass-physical properties.

LIBRARY
NAVAL POSTGRADUATE SCHOOL
MONTEREY, CALIF. 93940

TABLE OF CONTENTS

LIST OF TABLES

LIST OF ILLUSTRATIONS

ACKNOWLEDGEMENTS

The author wishes to thank Professors O. B. Wilson and R. S. Andrews for the guidance and encouragement provided by them for this research. The author also wishes to thank Professor R. Smith for his advice and the use of the vane shear apparatus, and Professor G. Griggs and his assistants of the Division of Natural Sciences, University of California at Santa Cruz, for the size and clay mineralogy analysis provided by them. Thanks are also due to Mr. K. Smith for his assistance in carrying out the measurements, and Mr. R. Moeller who helped to design and build much of the mechanical equipment used in this study. Financial support was received from the Foundation Research Program of the Naval Postgraduate School.

I. INTRODUCTION

Knowledge of the physical properties of ocean sediments has come into greater importance in recent years due to the need for a capability of predicting acoustic reflection characteristics of the ocean floor, which has become an essential part of modern sonar techniques, such as bottom bounce.

Various models of the ocean floor are being used to aid in these efforts. The simplest of these is the Rayleigh two-fluid model in which the sediment is considered to be another layer of fluid with a density and sound speed different than the overlying sea water. Although largely a successful model because of the low rigidity of most surficial sediments, the model predicts lower than observed bottom losses, especially at higher grazing angles (8). According to Morris (16), this is primarily due to neglect of the conversion of compressional wave energy into shear waves at the sediment interface and layer boundaries. For this reason a viscoelastic model is favored which uses complex Lame' constants and provides for the generation of shear waves upon reflection and for absorption of the waves (2).

This model shows good correlation with actual results in studies done by Bucker et al.(2) and Anderson and Latham (1) in which several sets of viscoelastic constants are assumed and solutions are correlated with observed data. Although it has been demonstrated to be feasible and accurate, the viscoelastic model presents the difficulty of evaluating

the Lame' constants for various oceanic areas and soft sediments. The only three direct methods known to be in use for evaluating them are by calculation from Stoneley wave velocities (10) or by use of torsional wave vibration (7) or a torsional wave viscoelastometer (4, 11).

The torsional wave viscoelastometer was demonstrated to be a feasible means for measuring the complex shear modulus or rigidity modulus of soft sediments at the Naval Postgraduate School by Hutchins (11). The method involves measuring the effects of shear waves generated in the sediment due to the propagation of torsional waves along the length of a round rod which is immersed in the sediment.

Hutchins experimented with laboratory prepared kaolinite-water mixtures in the frequency range of 38.3 to 38.9 kHz. Cohen (4), using an improved instrument of a similar design, extended the range of frequency to 5.8 to 38 kHz. Cohen obtained results from a study of a wide range of laboratory prepared kaolinite-water and bentonite-water mixtures. Results demonstrate that soft, undispersed, simulated sediments do have measurable shear moduli which are independent of frequency.

The purpose of the research described in this report was to develop and test a viscoelastometer suitable for in situ measurement and to apply it to the measurement of complex rigidity for a variety of samples of real ocean sediments. Although time did not permit inclusion of in situ measurements, the second goal was attained in these experiments. The following sections describe the theory of measurement,

the improved probe's construction, calibration procedures, sample collection and analysis procedures, the limitations of the method and results of the rigidity determinations. A discussion of the results and comparisons with other mass-physical properties are then presented.

II. THEORY OF MEASUREMENT

Use of a torsional mechanical oscillator as a viscometer has been described in detail by Mason (13), and McSkimin (15). This oscillator may be a crystal, ceramic, or ceramic-rod configuration resonating in a torsional mode. At mechanical resonance, a standing torsional wave exists along the axis of the system and the piezoelectric transducer which drives the system will have a maximum electrical conductance which depends upon the physical dimensions of the system and the properties of its constituents. Upon being immersed and making contact with a medium, shear waves are generated in the medium immediately adjacent to the system's surface and propagate radially outward. Although the shear waves in the sediment are usually too highly attenuated to allow investigation of their propagation, the radiation itself has a loading or damping effect on the system. This loading effect causes the resonant frequency and electrical conductance of the transducer to undergo a measurable change which is a function of the complex shear modulus of the medium. With properly evaluated constants of proportionality, the real and imaginary parts of the shear modulus can be determined.

Following Mason's development (13), if it can be assumed that the shear waves propagating radially outward into a fluid in contact with the surface of the rod have a wave-length which is very small compared to the radius of curvature of the rod, and that the amplitude

of these waves is rapidly attenuated, then the waves can be treated essentially as plane waves propagating in a fluid having a shear viscosity coefficient, η. For simple harmonic waves, the shear stress amplitude, T, for waves propagating in the z direction has the form:

$$T = T_o \exp - \left[\sqrt{\frac{\pi f \rho}{\eta}} (1 + j) z\right] , \qquad [1]$$

where the simple harmonic time term has been suppressed and where T_o is the initial stress amplitude, f is the frequency, and ρ is the fluid density. In a Newtonian liquid, the shear viscosity coefficient is $\eta = T/\dot{S}$, where S is the shear strain and $\dot{S} = \partial S/\partial t$ is thus the shear velocity. If one assumes that the medium is viscoelastic, η becomes complex (13) and

$$\eta_c = \eta_1 - j\eta_2 , \qquad [2]$$

where η_1 is the real part and η_2 the imaginary part of the shear viscosity coefficient. For a Newtonian fluid, η_2 is zero. This same phenomenon can also be described by a rigidity modulus, G, which is also complex:

$$G_c = G_1 + jG_2 , \qquad [3]$$

where G_2 is zero in a perfectly elastic solid and G_1 is zero in a Newtonian fluid. Since $\eta_c = T/j\omega\dot{S} = -j G_c/\omega$ for simple harmonic motion, where ω is the angular velocity,

$$G_1 = \omega\eta_2 \text{ , and } G_2 = \omega\eta_1 \text{ .} \qquad [4]$$

The impedance (Z) presented to the rod surface by the sediment is defined as the ratio of shear stress to shear particle velocity in an infinite medium as:

$$Z = R + jX = \sqrt{\pi f \eta \rho}\ (1+j) \text{ ,} \qquad [5]$$

where R and X are the specific acoustic resistance and reactance of the sediment, respectively. Substituting η_c for η in the equations relating η and G and separating real and imaginary parts yields:

$$\eta_1 = \frac{2RX}{\omega\rho} \text{ ,} \qquad \eta_2 = \frac{R^2 - X^2}{\omega\rho} \text{ ,} \qquad [6]$$

$$G_1 = \frac{R^2 - X^2}{\rho} \text{ ,} \qquad G_2 = \frac{2RX}{\rho} \text{ .} \qquad [7]$$

Thus, shear moduli or viscosities can be calculated by measuring R and X.

Mason (13) has shown that R and X are related to the change in resonant frequency, Δf, and the change in electrical resistance, ΔR_e, of the transducer driving the system by the equations:

$$\begin{aligned} \Delta R_e &= K_1 R_T \text{ ,} \\ \Delta f &= K_2 X_T \text{ ,} \end{aligned} \qquad [8]$$

where $R_T = R/L$ and $X_T = X/L$, [9]

and L is the length of the rod immersed. Values for K_1 and K_2 are obtained by measuring resonant frequency and electrical resistance with the rod in air, unloaded, and then loaded by immersion in one of several Newtonian liquids of known viscosity. Calculation of ΔR and Δf in Newtonian liquids therefore permits calculation of R and X, since $\eta_2 = 0$ and $R = X$. When K_1 and K_2 are known, measuring R and X in the sediment is reduced to measuring ΔR_e and Δf alone.

III. EQUIPMENT AND PROCEDURES

A. THE VISCOELASTOMETER

An improvement over those used by Hutchins and Cohen, the viscoelastometer used in this study is symmetrically driven by a transducer which generates torsional waves from a central location. The waves propagate up and down the rod made of two identical metal rod sections of the same diameter which are mechanically coupled to the transducer ends. Since the center of the transducer is a node for all torsional modes of vibration of the system, this is the most favorable location for the mechanical clamp which supports the system and the electrical leads to the transducer (Figure 1).

The driving transducer is a hollow barium titanate ceramic cylinder 0.5 inches in diameter and 1.5 inches in length. It is constructed from an axially polarized cylinder which is cut into two parts along the longitudinal axis and rejoined following inversion of one half section and insertion of two electrode grids (Figure 2). This produces a shear-type oscillation in the ceramic when electrically excited. A description of this method can be found in Mason (14).

This design, the location of the transducer at the center, a point of stress maximum for all resonant modes, improves the electromechanical coupling compared to an end transducer location. The arrangement is also suitable for total immersion and in situ measurement.

Based on recommendations in previous studies, a constant modulus alloy, NI-Span-C, was used for the rods. Both sections of the rod were heat treated and polished to a mirror-like finish.

The supporting structure of the viscoelastometer consists of a tubular steel frame welded to a contoured central clamp which is bolted together at the central node of the transducer to minimize any damping. Coaxial cable is drawn through the tubing of the outer supports through the central clamp to the mid-transducer electrodes. A covering with RTV insulating rubber and a thin neoprene rubber seal is added to insure the water tight security of the leads. The transducer is coated with GE-703-1 electrical varnish to accomplish complete electrical insulation. A removable spring-loaded screw atop the structure insures even application of stress to the rod during the process of insertion into the sediment.

B. RESONANCE METHOD

1. Equipment

The basic tool used to observe the transducer's electrical characteristics which are sensitive to the elastic properties of the sediment on the sidewalls of the viscoelastometer near resonance is the Dranetz Model 100B Impedance-Admittance Meter. Mechanical resonance occurs when the real part of the admittance is a maximum. Readings of this maximum admittance on the meter and the value of the

resonant frequency, read on a frequency counter, provided the necessary data for computation of sediment rigidity (Figure 4).

Since the viscoelastometer's performance is not entirely independent of temperature, all calibrations and measurements were made in a temperature controlled, water-jacketed pipe. The temperature of 9°C ± 0.1 C was maintained for all samples since this was the most common bottom water temperature observed at the sample collection sites.

2. Procedures in Measuring Rigidity

Calibration of the viscoelastometer as previously described was accomplished by measuring its resonant frequency and admittance while the probe was unloaded in air and then loaded in oils having known viscosities determined using a Brookfield Viscometer. These data permitted calculation of the quantities K_1 and K_2 referred to in equation [8].

All measurements were made in air and in the Newtonian oils at 9°C in the water-jacketed pipes. In each case, 5 or 6 hr were allowed to insure that thermal equilibrium had been attained. The three oils used, whose viscosities covered a wide range, were: motor oil (4.58 poise), Brookfield Standard silicone oil (12.53 poise), Brookfield Standard silicone oil (162.0 poise).

For each resonant mode, average values of the constants were computed from the measurements in the three fluids. Useful

resonances occurred at 4.3, 15.3, 25.6, and 35.1 kHz for half the measurements. After the original transducer was replaced, these useful resonances occurred at 4.4, 27.2, and 38.6 kHz.

Prior to inserting the viscoelastometer into the sediment samples, a smaller diameter hollow rod was pushed into the sediment and withdrawn to reduce the stress placed upon the probe upon insertion. After the probe was pushed into the sediment, a thermistor probe was inserted into the sediment between the rod and sediment core liner. The core and probe were placed into the water-jacketed pipe and allowed to attain temperature equilibrium before measurements were made.

C. THE SAMPLES

The samples used in this experiment were all continental terrace sediments obtained during two cruises on the U.S.N.S. BARTLETT (T-AGOR-13). Cruise One in Monterey Bay was completed in November 1969. Cruise Two was completed in February 1970. The samples were retrieved by gravity corers, Shipek grab samplers and pipe dredges. Rigidity measurements on the gravity core samples, designated by the prefix "G" in Tables 1 and 2, were carried out in their core liners. Shipek grab samples and pipe dredge samples, designated by the prefix "C" in Tables 1 and 2, were remolded into core liners before the measurements were made. The core liners had an inside diameter of 2.5 inches in all cases. Gravity cores longer than 14 inches were cut into 14-inch sections and are labeled with consecutive Roman numerals

in Tables 1 and 2. These cores were stored at 2°C, immersed in bags of seawater to reduce biological activity and prevent dessication. Locations of the collection sites are listed in Table 1.

D. COMPRESSIONAL WAVE SPEED

1. Equipment

The compressional wave or sound speed in the samples was measured by determining the time delay for a short sound burst through a known length of the sediment. Two barium titanate disk transducers were used, one as the transmitter, the other as receiver. Measurements were made at a frequency of 2 MHz, the resonant frequency for the transducers. A sketch of the apparatus is shown in Figure 3. Other apparatus included a dial indicator, a dual beam oscilloscope, a pulsed oscillator, a time mark generator, and an amplifier.

2. Procedures

A calibration check of the velocimeter system was accomplished by making measurements in a 22% ethanol, 78% water mixture rather than pure water in order to reduce the temperature dependence of the sound speed (17).

A 2- to 3-inch section of core was cut and placed into the sound velocimeter well. Temperature was monitored and kept very near to 9°C. Several measurements were made by matching echos and determining time delay on the dual beam oscilloscope. These values were averaged and corrected to 9°C when necessary. They were later

compared with seawater sound speeds calculated at 9°C and 35 0/00 salinity (12) in order to determine ratios of the sound speed in the sediment to that in seawater.

E. VANE SHEAR TEST

1. Equipment and Procedures

Shear strength measurements were obtained by a motorized Wykeham-Farrance vane shear machine. A 2.5-inch long core was taken from each sample and placed securely into the machine. One-inch by one-inch vanes were used with a shaft rotation rate of 1 rev/hr. The vane was inserted 1 inch deep into a section of each core, the motor was started and torque was applied gradually to the sediment by means of a spring connecting the shaft to the motor. Calculation of the shear strength was obtained by noting the angular deflection at the precise time the sediment was observed to have sheared using the equation:

$$S = \frac{M}{\pi D H \frac{D}{2} + \frac{2 \pi D^2}{4} \frac{2}{3} \frac{D}{2}} \quad , \qquad [10]$$

where H is vane height, D is vane diameter, and M is a spring calibration figure depending on the angle of deflection at shear (3). These vane shear tests were run also at 9°C.

F. SAND-SILT-CLAY RATIOS: MINERALOGY

Sand-silt-clay ratios and clay mineralogy were determined by the Division of Natural Sciences of the University of California at Santa Cruz.

The settling tube method was used for size analysis and an X-ray diffraction method was used to obtain the mineralogy by percentages.

G. WET DENSITY AND POROSITY

Wet density is measured by weighing a known volume of water-saturated sediment. Porosities are obtained by placing the sample used to determine density in an oven at 105°C for 24 hr. At the end of the 24-hr period, the weight is again measured. Assuming that the lost weight is entirely water, and further assuming that 1 ml of water weighs 1 g, the volume of water per unit volume is computed.

H. CALCULATED PARAMETERS

Shear wave speed, Poisson's ratio, and the product of density and sound speed squared were calculated by computer. The shear wave speed, C_s, is calculated using the formula:

$$C_s = \sqrt{G/\rho} \quad , \qquad [11]$$

where G is absolute value of the complex rigidity and ρ is the wet density. Poisson's ratio, δ, is calculated using the equation:

$$\delta = \frac{1}{2} \left(1 - \frac{1}{((C/C_s)^2 - 1)} \right) \quad , \qquad [12]$$

where C is the compressional sound speed (6). The measured and computed physical and acoustic properties of the marine sediments are shown in Table 2.

IV. LIMITATIONS OF THE METHOD

A pair of assumptions made in the development of equation [1] for the resonance method are that the wave length of the shear wave in the medium is very much smaller than the radius of curvature of the rod and that the amplitude of this wave decays to a small value in a distance small compared to the radius of the rod. Calculations of the wave lengths for the stiffer samples at the lowest frequency used indicate that this assumption is no longer valid. Therefore some of the results at 4.4 kHz may be in error. The assumption is fulfilled at all the other higher frequencies.

A second limitation of the probe for this experiment results from the fact that the probe constants, K_1 and K_2, are not constant over a wide range of viscosities. In earlier experiments, the probe was calibrated in fluids in which the viscosity ranged from 1 to 5 poise. In this experiment, a much wider range of viscosities, 5 to 160 poise was used; values for K_1 and K_2 were not constant (Table 3). Average values of the constants were used to compute the rigidities.

No estimate is made of the effects of the invalidity of the assumptions on accuracy of the rigidity values. There is, however, some question about the absolute accuracy of the results at the lowest frequency in the stiffer sediments.

The effect of averaging the calibration constants determined from the different fluids is easily estimated. An error analysis using these averaged constants yielded a maximum absolute error of 40% in the real component of rigidity, G_1, and 125% in the imaginary component of rigidity, G_2. This high degree of error stems almost entirely from the variation of the constants.

The effects of the result due to uncertainties of the constants individually and the standard deviations of the frequency and conductance measurements yield a maximum relative error of about 6% in G_1 and from 40 to 90% in G_2. This large error in G_2 results from the fact that it is primarily determined by the change in resonant frequency. Since these changes are sometimes comparable to the precision of measurement of the change in frequency, a large fractional error can result. A suggested improvement for future calibrations is that a narrow range of high viscosity oils be used for the best constants.

A third limitation of the viscoelastometer is its anomalous behavior in very sandy sediments. When the percentage of sand exceeds 50%, all resonant modes change in resonant frequency in the opposite direction from that expected. The reason for this behavior is not fully understood but is believed to result from the fact that the particle size of the sand in contact with the viscoelastometer is of the same magnitude as the shear wave length and therefore, the assumption of a uniform medium is not valid. This belief is supported by observations that the anomalous

behavior occurred at lower sand concentrations for the lowest frequency modes, for which the wave length was greatest.

V. RESULTS AND DISCUSSION

The results of the experimental measurements and analysis are presented in Table 2. In order to study these data, it seems worthwhile to use a graphical method. There follows below a description and discussion of the graphical comparisons between the observed quantities.

It is necessary in comparing these data that recognition be given to some of the limitations. Such limitations concern the viscoelastometer, the samples and sampling methods.

The viscoelastometer, although capable of total immersion in salt water, was not used as originally intended, an in situ probe. The reason for this is the temperature dependent properties of the rod's performance and calibration constants which require the use of temperature controlled laboratory conditions. Its anomalous behavior in very high sand concentration sediments relegates its use to softer clay or silt sediments retrieved from the ocean bottom. This restriction to retrieved sediments must be noted, for the samples measured were subjected to considerable structural damage in the case of gravity cores and to massive, if not total, structural damage in the case of remolded cores from Shipek samplers or pipe dredges. This fact must be kept in mind in any evaluation or rigidities calculated in this study.

The magnitude of the real component of rigidity observed in these surficial continental terrace clayey-silt sediments range from 6.5×10^5 to 2.6×10^7 dynes/cm^2. Measurements of the imaginary components

of rigidity range between 2.9×10^5 and 8.2×10^6 dynes/cm^2. Corresponding shear wave speeds calculated from these data are between 7 and 40 m/sec. The magnitudes of the rigidity observed in this study are less than those in the findings of Hamilton et al. (10), who found a value of 1.6×10^8 dynes/cm^2 for sediment of this nature off San Diego, using the Stoneley wave techniques. This difference in magnitude could be related to three factors: (a) Monterey Bay sediments have been recently laid down at high deposition rates, allowing little time for cementation and/or compaction; (b) as mentioned above, the rigidity could have been reduced due to disturbance or damage to the sediment by the sampling methods; (c) the Stoneley wave technique may be affected by at least the first meter of sediment, yielding an averaging of the rigidities in this meter of depth. The literature, however, is not devoid of results confirming the existence of possible low rigidities. Anderson and Latham (1), in a study of the dispersion of seismic Rayleigh waves, assume a shear velocity gradient of 30 to 190 m/sec for the top 150 m of sediment and find good correlation between observed and calculated results. A similar study done with explosively generated Stoneley waves on the ocean bottom by Davies (5) shows a shear wave speed of 50 m/sec in the surface layers. Such shear wave speeds would yield rigidities on the order of those observed in this study. Gallagher and Nacci (7), using a torsional wave vibration method, arrive at a value of 2.3×10^7 dynes/cm^2 for sediments of a nature similar to that of the stiffer sediments in this report. However, the

wealth of information available on this subject reports somewhat higher shear wave speeds requiring correspondingly higher rigidities (9).

In addition to rigidity, other physical properties were measured or calculated for the samples (Table 2). These include density, porosity, compressional sound speed, shear wave speed, vane shear strength, sand-silt-clay ratios, montmorillonite, illite, chlorite percentages, the ratio of the sound speed in the sediment to that in seawater, Poisson's ratio and the product of density and sound speed squared, ρc^2. Most of these properties are graphically compared with both real and imaginary components of rigidity in the following sections.

The real component of rigidity, G_1, does exhibit several interesting trends when related to certain physical properties. As can be seen from graphs of G_1 against density (Figure 5) and against porosity (Figure 6), G_1 tends to increase with increasing density and decreasing porosity. This result is not surprising and has been explained by Hamilton (9). Higher porosities lead to lower densities and lower rigidities due to fewer interparticle contacts in sands and clayey silts. Rigidity increases with increasing density may also be the normal result of compaction which tends to increase both properties. The real component of rigidity, however, shows no clear relationship with sound speed in the sediments (Figure 7).

In comparing rigidity to percentages of sand (Figure 8), silt (Figure 9), and clay (Figure 10), no consistent relationships with

percent sand or percent silt seem to be apparent. However, a general trend of increasing G_1 with decreasing clay content is visible in Figure 10. Hamilton (9) also observes this trend in abyssal plain and hill sediments and considers the clay fractions as a good index to rigidity in this region.

Plots were made of rigidity as a function of the relative amounts of montmorillonite (Figure 11), illite (Figure 12), and chlorite (Figure 13). The graphs reveal that the relationship between montmorillonite and rigidity is unclear, that illite content was fairly constant for the samples and that increasingly rigid samples appear to have increased amounts of chlorite clay. Hamilton (9) states that mineralogy changes can indeed affect rigidity due to size differences and different inter-particle bonding.

Vane shear tests results (Figure 14) correlate surprisingly well with the rigidity. Although the value of vane shear measurements appears to be held somewhat in question by both soil engineers and geologists, the relationship observed in this report at least adds some credibility to the value of vane shear measurements and it suggests the properties which determine shear strength or the cohesion of a sediment may also influence its rigidity.

Comparisons were also made between rigidity and the calculated parameters. Figure 15 indicates that G_1 tends to increase with an increase of ρc^2. This trend is in agreement with the findings of Hamilton (9) who considers this to be a good index for rigidity in the

continental terrace sediment region. Since density, rigidity, and sound speed were used in computing Poisson's ratio, the graph of G_1 as a function of Poisson's ratio (Figure 16) shows only that measurements of these three properties are self-consistent. Poisson's ratio for all samples was approximately 0.5. This value is comparable to values reported by Hamilton et al. for clayey silts (10).

Thus, it appears from the above discussion and graphs that relationships exist between rigidity determined by this method and density, porosity, clay content, ρc^2, clay mineralogy and vane shear strength. It is also logical to assume that rigidity, density, porosity and ρc^2 for these samples are all interrelated and affect the rigidity collectively. It would appear that the real component of rigidity is related to density and porosity, which are determined primarily by compaction and interparticle contact, and to other physical properties, clay content, mineralogy, and shear strength, which are related to structure and interparticle bonds. The influence of cementation and rate of deposition remain unmeasured in this study and may be the cause of some of the wide scatter observed on the graphs. Hamilton also notes that the widest scatter for physical properties and rigidity exists for continental terrace sediments (9).

The imaginary component of rigidity, G_2, related to mechanical or anelastic losses in the sediment, when graphed against various physical properties exhibits few visible trends. A possible contributor to this is the fact that the precision of measurement for G_2 with this

method is somewhat less than for G_1. In general, it can be said that G_2 shows no relationships with density, porosity, sound velocity, vane shear strength, percent sand, percent illite and ρc^2. However, when remolded samples are differentiated from gravity cores, two separate trends appear on some of these graphs, one for remolded samples and one for gravity cores. With this differentiation, trends appear to exist for density, porosity, vane shear strength, percent sand and ρc^2. The graph of G_2 as a function of density (Figure 17) reveals only a wide scatter of points. However, if the nature of the samples is considered, an unexpected but persistent trend seems to be apparent. For remolded samples, it appears that G_2 increases with increasing density. A less well-defined trend indicating a more rapid increase of G_2 with increases in density is indicated for the gravity core samples. When the imaginary component of rigidity is graphed against porosity (Figure 18), only remolded samples appear to show a consistent trend. No consistent relationship between G_2 and the compressional sound speed seems to be indicated in Figure 19.

Graphical plots of the values of G_2 as a function of percentages of sand (Figure 20), silt (Figure 21), and clay (Figure 22), show no clear relationship with increasing sand or silt content. However, the imaginary component of rigidity does vary inversely with clay content.

The imaginary part of the rigidity is apparently affected by the mineralogy of the clays involved; G_2 appeared to increase with corresponding decreases in the amount of montmorillonite (Figure 23), and

with increases in the chlorite content (Figure 25). This trend exists for both remolded and gravity core samples. This is not surprising as mineralogy affects rigidity by differences in interparticle bonds and particle sizes. Illite remained somewhat constant for all samples and G_2 showed no dependence with illite (Figure 24). This variation of G_2 with clay mineralogy is a possible indication that internal losses are affected largely by the type of sediment structure.

Vane shear results (Figure 26) show a trend of G_2 increasing with increasing cohesion, with several inconsistencies. This reinforces the indication that the imaginary component of rigidity is determined by properties related to the cohesion and structure.

When graphed against ρc^2 (Figure 27), two separate trends again appear for remolded and gravity cores, with G_2 increasing with ρc^2 for both. This is a trend similar to that shown by G_1, the real component of rigidity.

The imaginary component of rigidity shows a reasonably good relationship with Poisson's ratio (Figure 28), but again this is an indication of the consistency of our measurements and computations.

The graphical presentations here show weak relationships between G_2 and density, porosity, vane shear strength, percent sand and ρc^2 It must be noted, however, that these trends are observed only when remolded samples are differentiated from gravity core samples. More readily apparent relationships are observed between the imaginary component of the rigidity and the presence of the clay minerals montmorillonite

and chlorite in the samples. Because of this anomalous and weak dependance of G_2 upon the physical properties, and the observed dependance on clay mineralogy and percent clay, it might be inferred that G_2 is more dependent on a factor related to the clay content or the structure of this clay. Since the primary difference between a remolded sample and a gravity core sample is the massive destruction of the original sediment structure in the former and since the G_2 values were lower on the whole for the remolded samples, these results suggest that the imaginary component is highly influenced by factors preserved by the original structure.

Although values of both the real and imaginary components of rigidity, G_1 and G_2 respectively, do tend to vary with frequency, no consistent or definite pattern of frequency dependence of either the real or imaginary components of rigidity is observed. Typical values of G_1 and G_2 and their variation with frequency are presented for six samples in Figures 29 and 30.

VI. CONCLUSIONS AND RECOMMENDATIONS

It is concluded that the torsional wave probe method used in the experiments reported here is probably giving valid results for the rigidities for the following reasons: (a) the values of the real parts of the rigidity determined seem to compare reasonably well with the order of magnitudes reported by other workers using other methods on soft sediments; and (b) the dependence of the results on some of the mass-physical properties seems to be consistent with the work of the others.

Because of this and because the method also yields a value for the imaginary component of the rigidity, which should pertain to the sound absorption process, it suggests that this method may be useful as a tool for sediment analysis and that it should be developed further. It is important that the method be validated by independent measurements in the same material using another method, such as the Stoneley wave method. The relationships between rigidity and other physical properties, especially clay mineralogy, need further investigation.

SAMPLE	LATITUDE	LONGITUDE	METHOD
G-1 Section I (top)	36° 51.2'N	121° 57.9'W	G.C.
G-1 Section II			
G-1 Section III			
G-1 Section IV (Bottom)			
G-2	36° 48.2'N	122° 00.2'W	G.C.
G-5	36° 41.5'N	121° 53.9'W	G.C.
G-6	36° 46.4'N	121° 56.0'W	G.C.
G-8	Unknown		G.C.
G-10 Section I (top)	36° 47.9'N	121° 51.5'W	G.C.
G-10 Section II			
G-10 Section III (bottom)			
G-12	36° 49.3'N	121° 57.5'W	G.C.
G-13 Section I (top)	36° 14.1'N	123° 22.4'W	G.C.
G-13 Section II (bottom)			
C-2	35° 51.2'N	121° 57.9'W	S.S.
C-5	36° 41.5'N	121° 53.9'W	S.S.
C-6	36° 41.4'N	121° 56.0'W	P.D.
C-7	36° 41.4'N	121° 56.0'W	P.D.
C-8	35° 47.0'N	123° 13.2'W	P.D.
C-9	35° 47.0'N	123° 13.2'W	P.D.

G.C. - Gravity Core
S.S. - Shipek Sampler
P.D. - Pipe Dredge

TABLE 1. Positions of Sampling Sites

SAMPLE	G-1 10^6 dynes/cm^2	G-2 10^6 dynes/cm^2	DENSITY g/cm^3	POROSITY %
1. G-1 Section I	1.5	0.73	1.44	72.6
2. G-1 Section II	6.0	2.2	1.42	72.9
3. G-1 Section III	11	4.7	1.50	69.5
4. G-1 Section IV	13	5.7	1.48	71.0
5. G-2	26	7.1	1.63	66.0
6. G-5	8.8	4.9	1.52	71.9
7. G-6	6.8	2.2	1.46	75.3
8. G-8	2.2	1.3	1.42	73.9
9. G-10 Section I	7.6	3.5	1.43	72.5
10. G-10 Section II	9.1	5.3	1.50	76.0
11. G-10 Section III	15	8.2	1.60	64.0
12. G-12	20	1.7	1.64	55.7
13. G-13 Section I	12	6.5	1.34	79.1
14. G-13 Section II	7.3	5.1	1.37	76.5
15. C-2	3.5	1.8	1.42	73.1
16. C-5	3.1	1.0	1.60	66.2
17. C-6	17	2.8	1.67	58.6
18. C-7	13	3.1	1.76	53.2
19. C-8	0.95	0.54	1.38	73.6
20. C-9	0.62	0.30	1.34	74.2

TABLE 2. Tabulated Physical Properties

SAMPLE NUMBER	SHEAR WAVE SPEED m/sec	COMPRESSIONAL WAVE SPEED m/sec	Csed/ Cwater	VANE SHEAR STRENGTH lb/in^2
1.	10.8	1476.7	0.992	0.12
2.	21.1	1481.9	0.996	0.18
3.	27.9	1495.2	1.005	0.40
4.	31.1	1462.7	0.982	0.40
5.	40.3	1484.3	0.999	1.70
6.	25.7	1484.2	0.999	0.30
7.	22.1	1499.3	1.003	0.44
8.	13.5	1415.6	0.951	2.50
9.	24.1	1462.6	0.983	0.36
10.	26.0	1478.4	0.993	0.32
11.	33.0	1487.1	1.001	0.42
12.	35.4	1532.9	1.030	1.71
13.	32.3	1459.6	0.982	0.51
14.	25.5	1459.9	0.981	0.40
15.	16.6	1456.3	0.979	0.12
16.	14.2	1489.3	1.002	0.23
17.	32.0	1467.5	0.987	0.73
18.	27.4	1463.1	0.984	0.73
19.	8.8	1462.4	0.983	0.12
20.	7.1	1478.0	0.992	0.10

TABLE 2. Tabulated Physical Properties (Cont.)

SAMPLE NUMBER	SAND %	SILT %	CLAY %	MONTMORILLONITE %	ILLITE %	CHLORITE %
1.	0.6	83.7	15.1	70	16	14
2.	0.3	85.5	14.2	65	15	20
3.	0.7	85.7	13.6	60	10	22
4.	0.0	86.9	13.1	69	16	15
5.	---	---	---	--	--	--
6.	5.3	81.0	13.7	--	--	--
7.	1.3	69.1	29.6	76	12	12
8.	34.2	53.7	16.1	71	16	13
9.	1.6	89.0	9.4	64	20	16
10.	8.7	84.5	6.8	57	13	30
11.	15.1	76.3	8.6	70	11	19
12.	36.4	57.0	6.6	77	13	10
13.	3.1	72.9	24.0	48	26	26
14.	2.2	86.7	11.1	55	31	14
15.	0.4	82.7	16.7	68	15	17
16.	8.0	80.7	11.3	66	20	14
17.	44.0	44.2	11.8	35	32	33
18.	36.5	51.1	11.4	67	19	14
19.	20.7	55.5	23.8	94	2.4	3.4
20.	4.1	70.6	25.2	75	16	19

TABLE 2. Tabulated Physical Properties (Cont.)

SAMPLE NUMBER	ρc^2 (10^6 g-m^2/cm^2-sec^2)	POISSON'S RATIO
1.	3.14	0.499_{97}
2.	3.12	0.499_{90}
3.	3.35	0.499_{83}
4.	3.17	0.499_{77}
5.	3.60	0.499_{94}
6.	3.35	0.499_{89}
7.	3.28	0.499_{82}
8.	2.06	0.499_{76}
9.	3.06	0.499_{98}
10.	3.41	0.499_{99}
11.	3.54	0.499_{96}
12.	3.85	0.499_{63}
13.	2.87	0.499_{85}
14.	2.92	0.499_{95}
15.	3.01	0.499_{73}
16.	3.55	0.499_{86}
17.	3.60	0.499_{85}
18.	3.77	0.499_{76}
19.	2.95	0.499_{76}
20.	2.93	0.499_{85}

TABLE 2. Tabulated Physical Properties (Cont.)

OIL	K_1	K_2
MOTOR OIL	3.36	0.0025
SILICONE OIL (12.53 poise)	3.10	0.0015
SILICONE OIL (162 poise)	1.57	0.0003

TABLE 3. Variation of Constants at 4 kHz

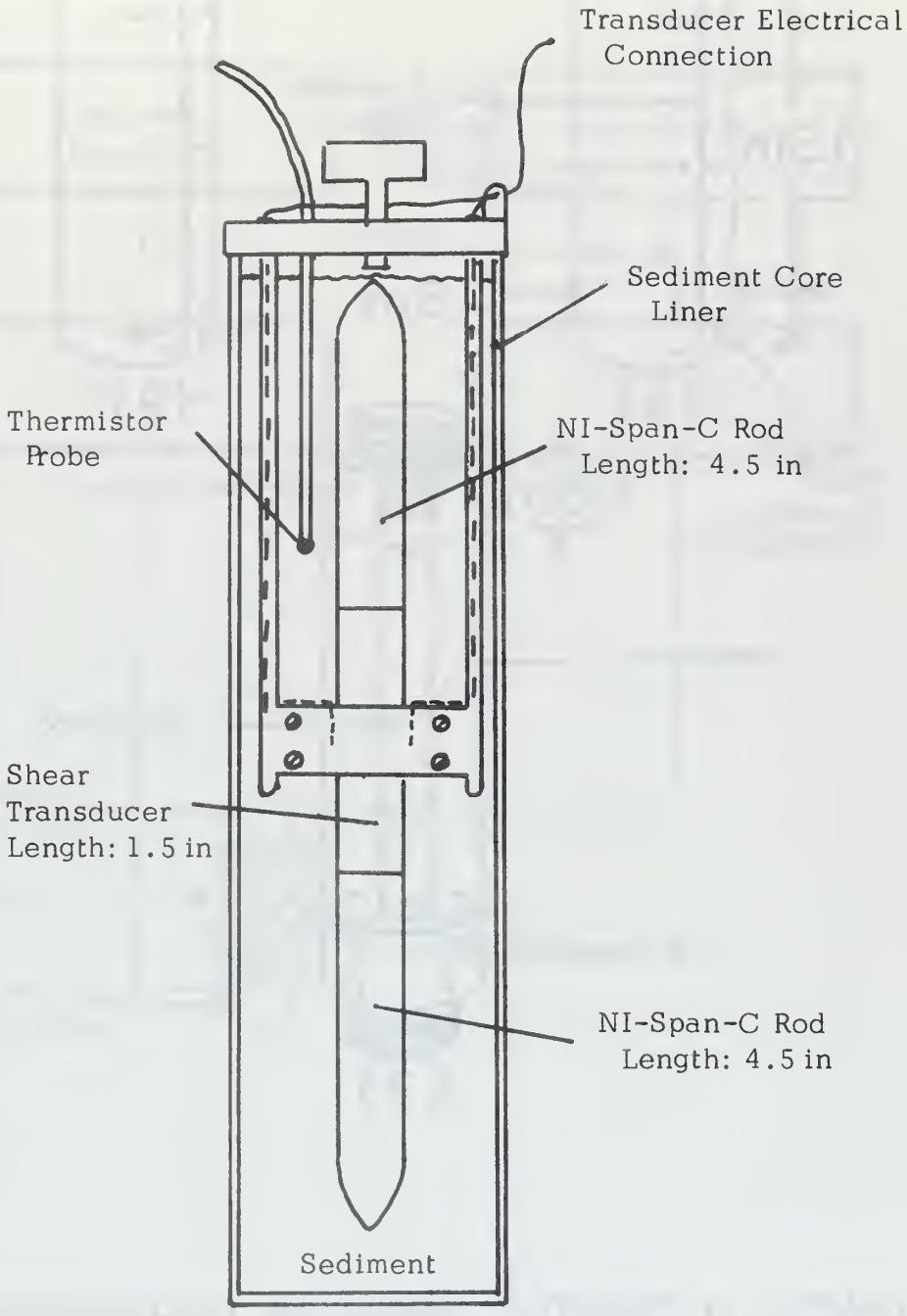

FIGURE 1. CUT-AWAY VIEW OF THE SYMMETRICALLY DRIVEN VISCOELASTOMETER AND SAMPLE.

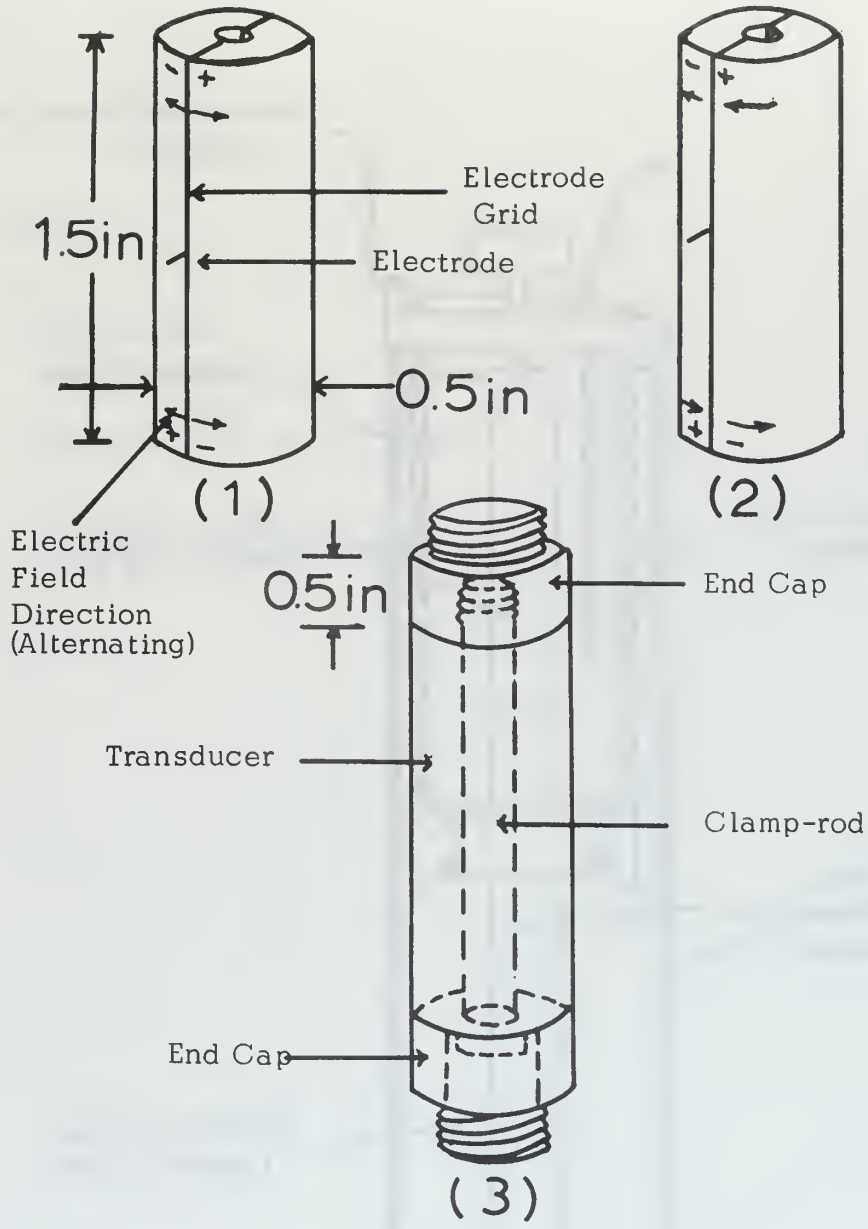

FIGURE 2. (1) POLARITY OF TRANSDUCER, FIELD DIRECTION, (2) SHEAR STRESS DIRECTIONS, (3) MODE OF COUPLING.

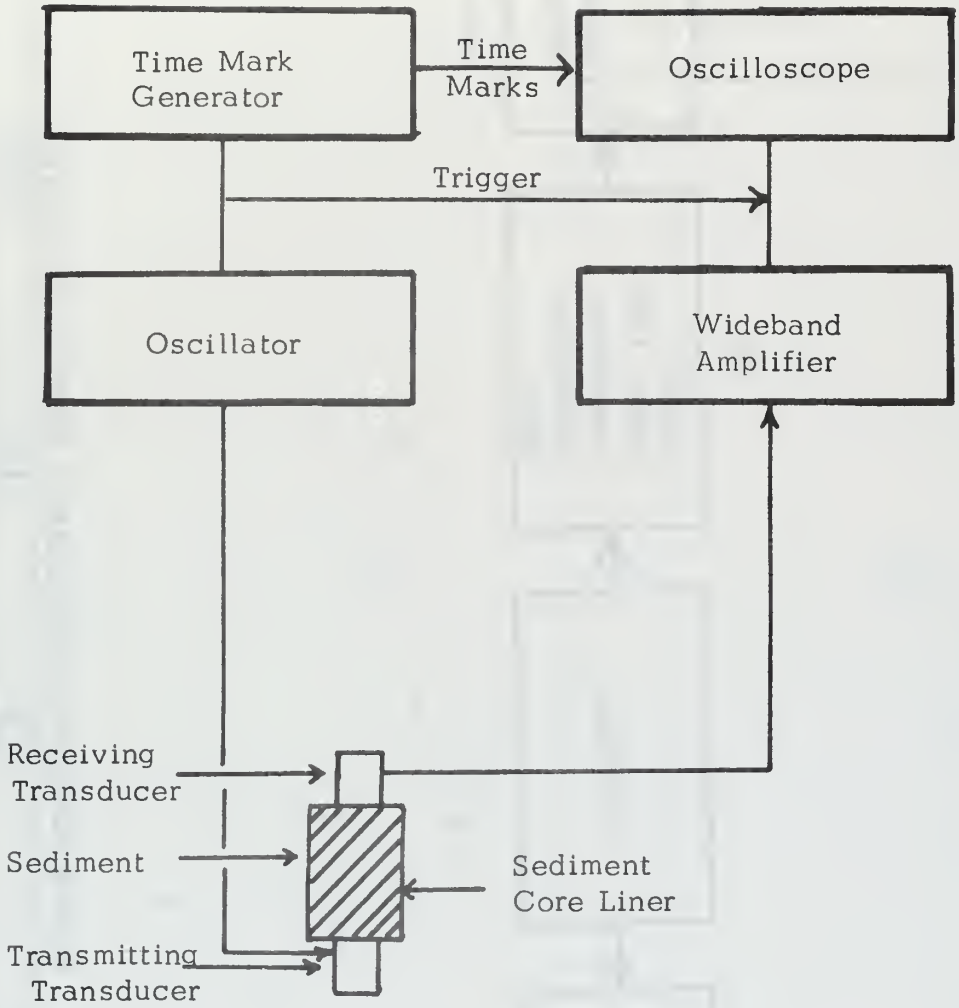

FIGURE 3. SOUND VELOCIMETER AND BLOCK DIAGRAM FOR ITS OPERATION.

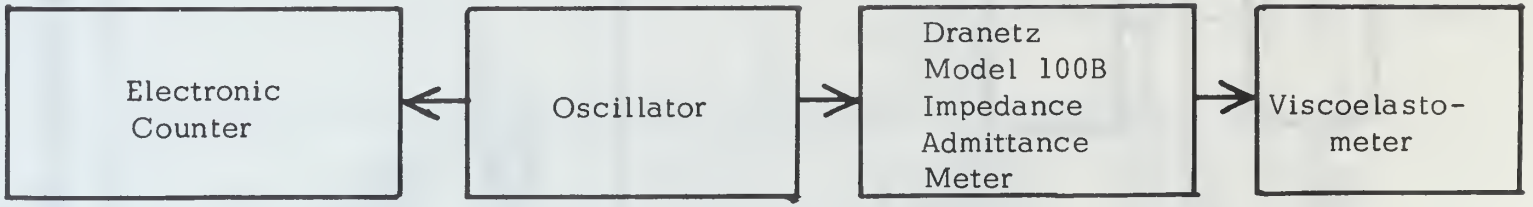

FIGURE 4. BLOCK DIAGRAM OF RESONANCE METHOD EQUIPMENT

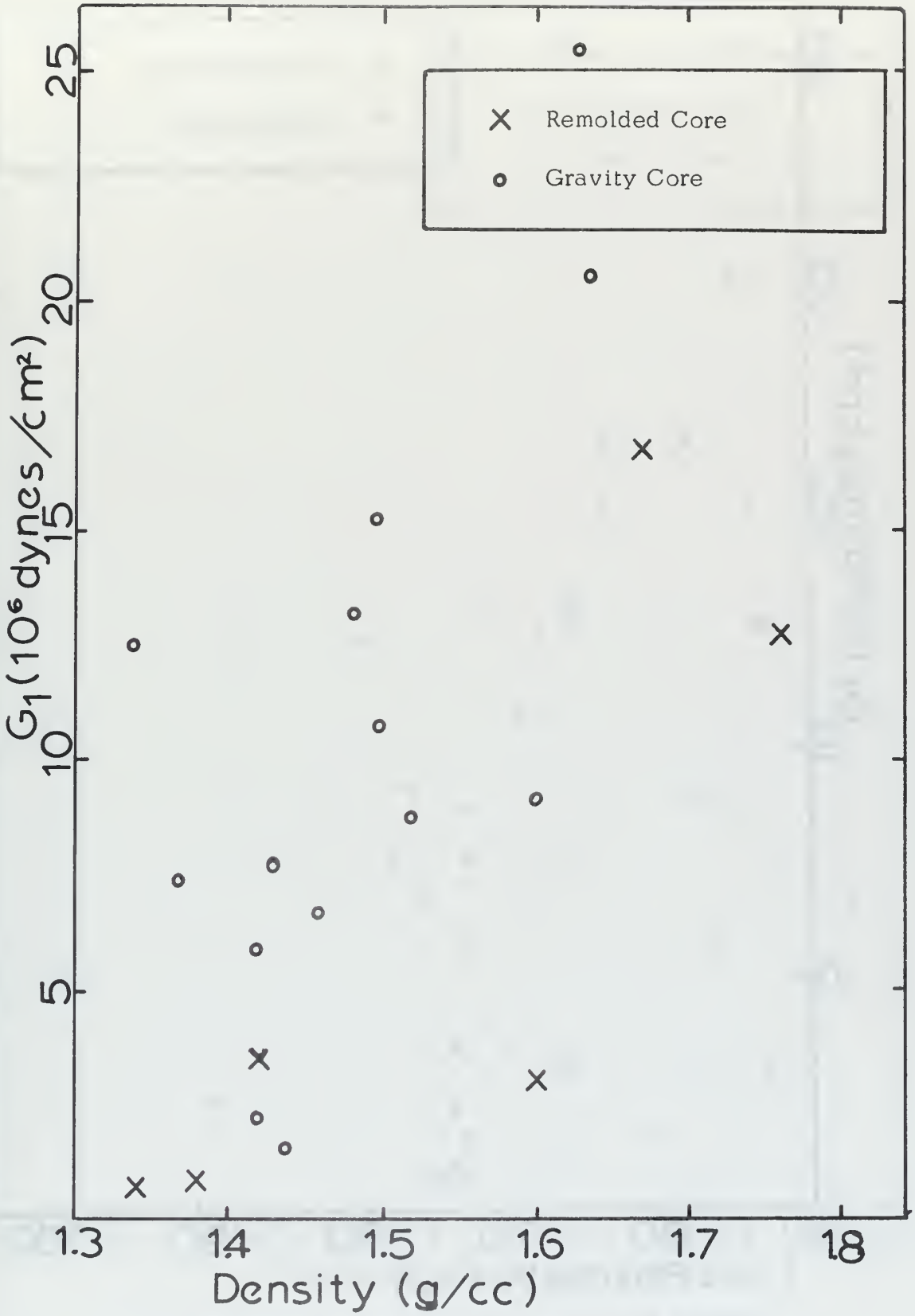

FIGURE 5. G_1 AS A FUNCTION OF DENSITY.

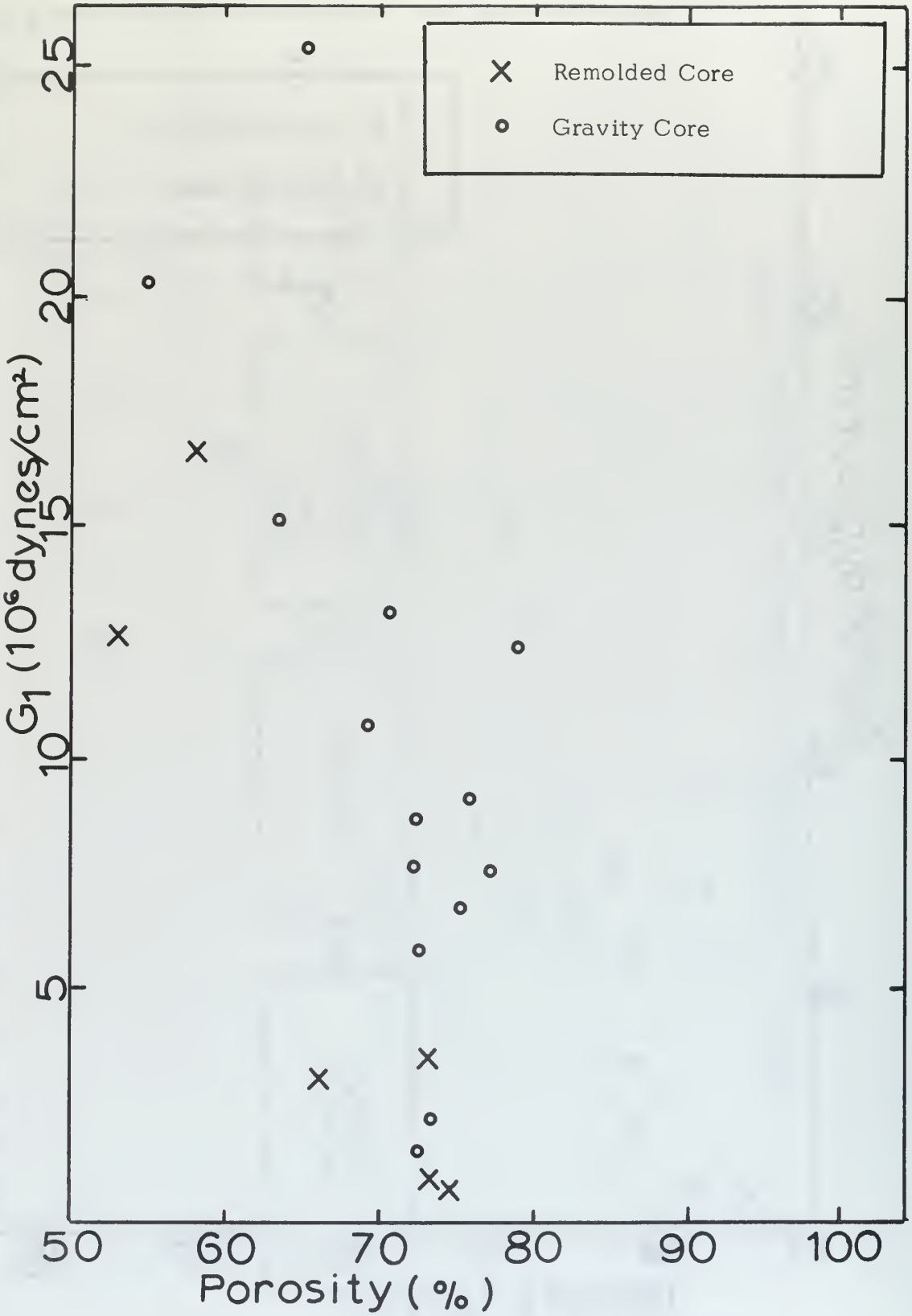

FIGURE 6. G_1 AS A FUNCTION OF POROSITY.

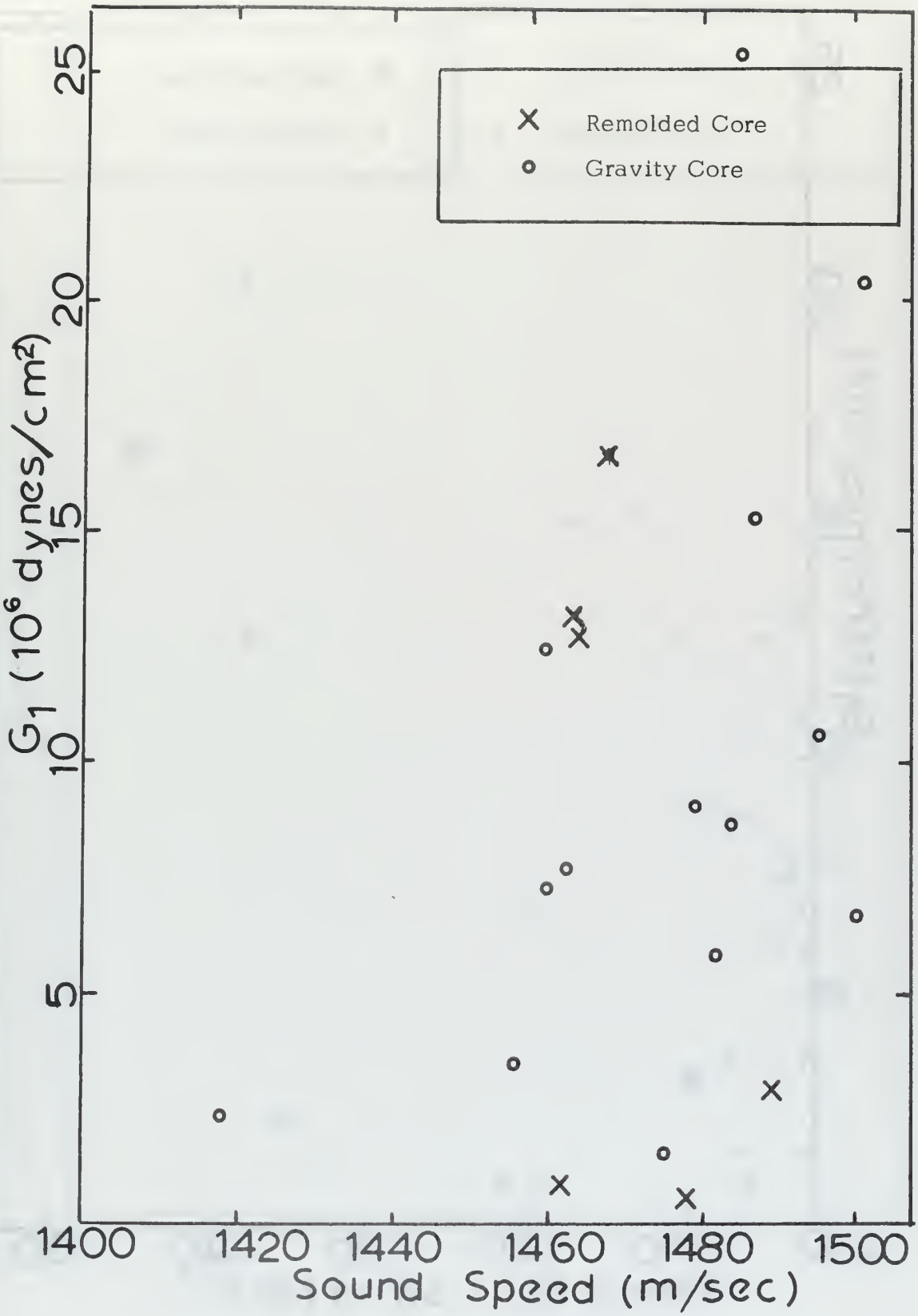

FIGURE 7. G_1 AS A FUNCTION OF SOUND SPEED.

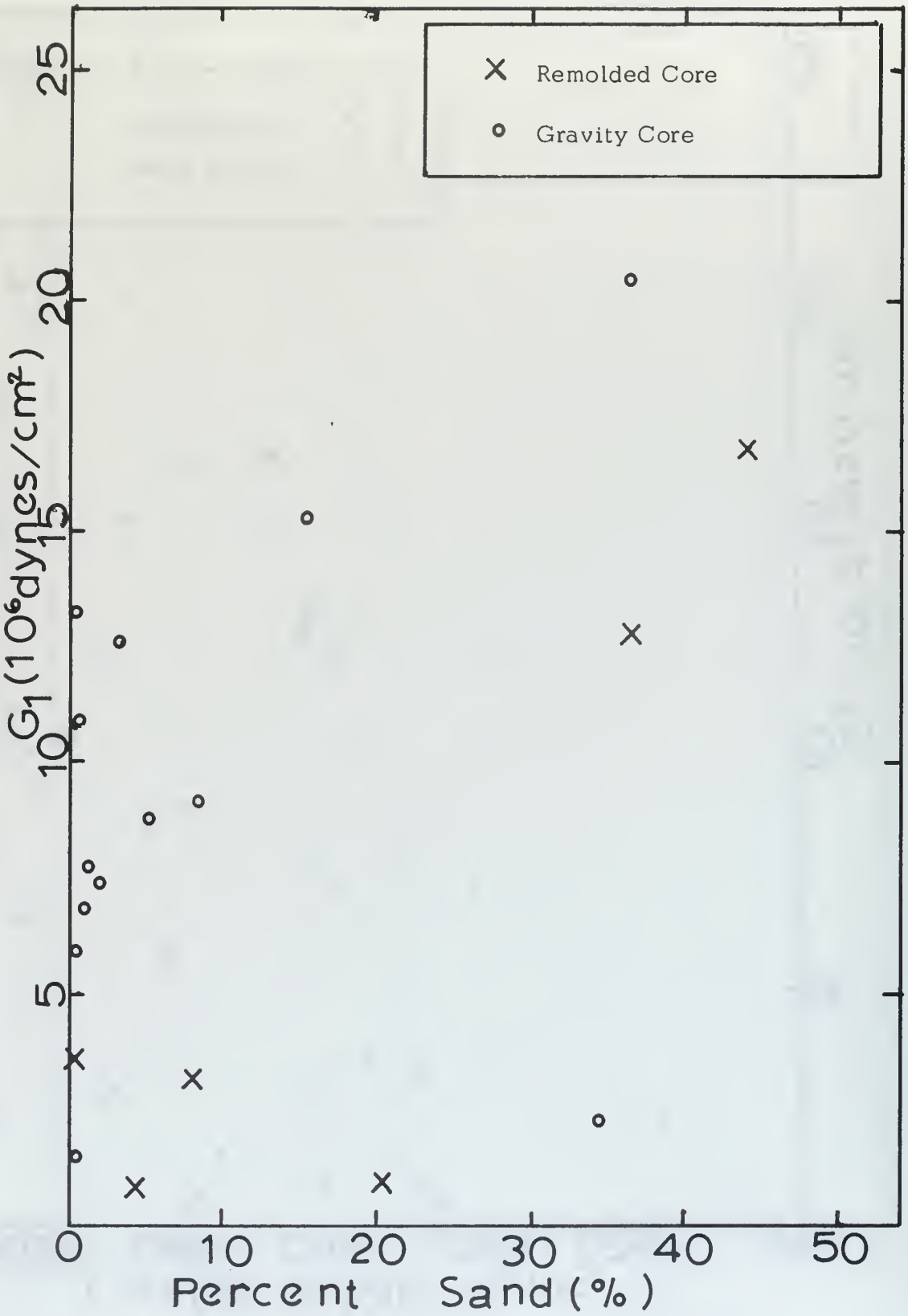

FIGURE 8. G_1 AS A FUNCTION OF PERCENT SAND.

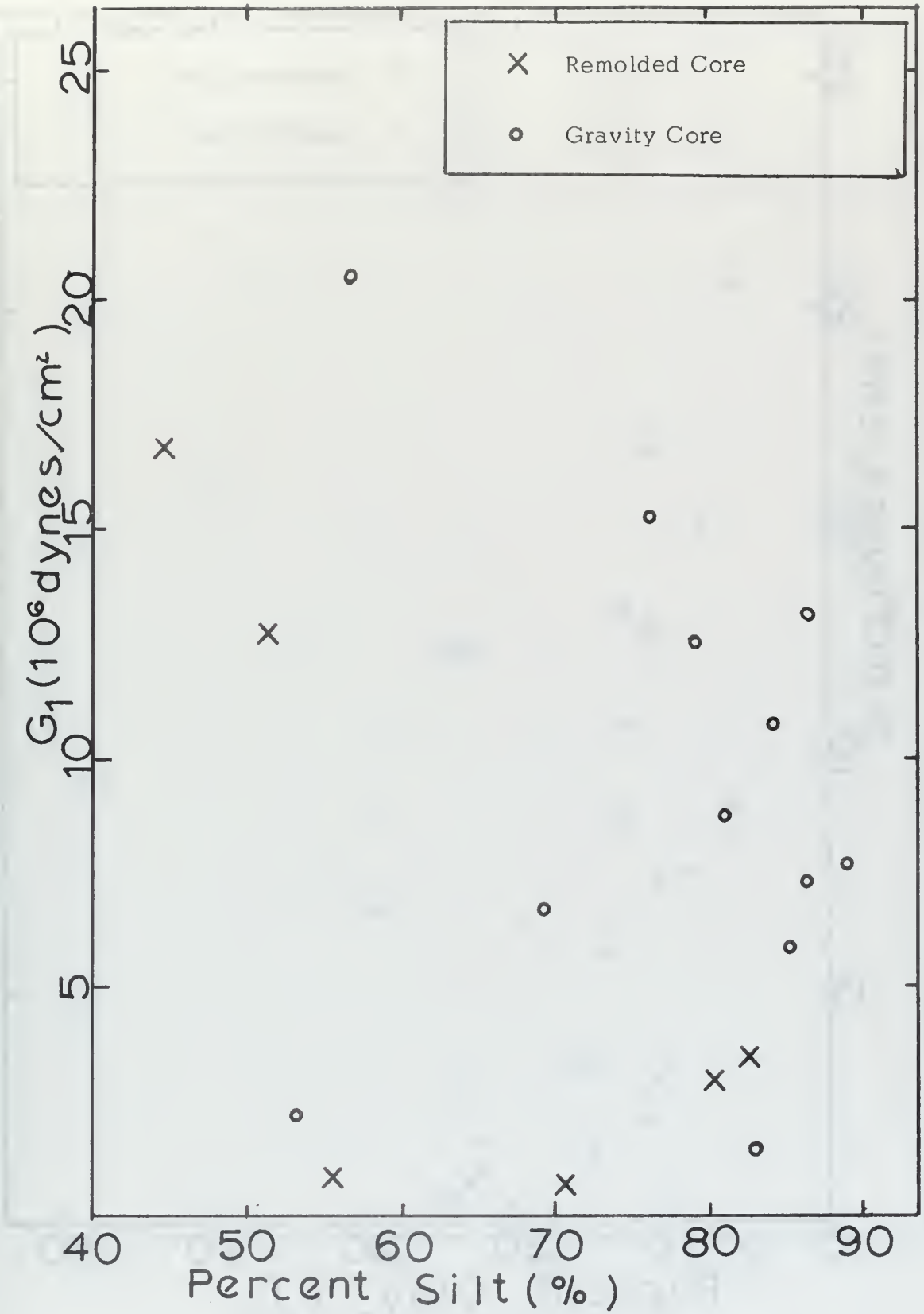

FIGURE 9. G_1 AS A FUNCTION OF PERCENT SILT.

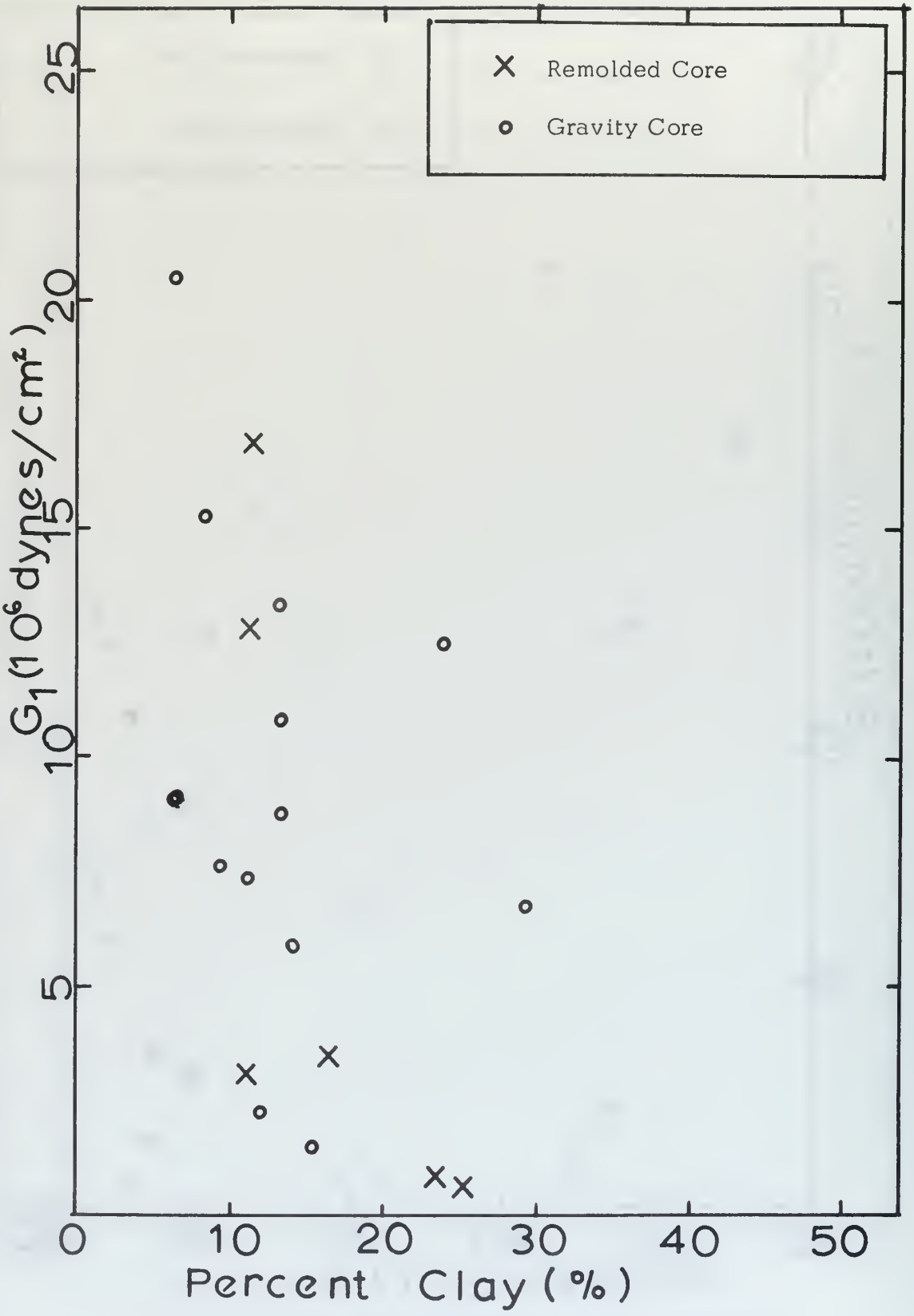

FIGURE 10. G_1 AS A FUNCTION OF PERCENT CLAY.

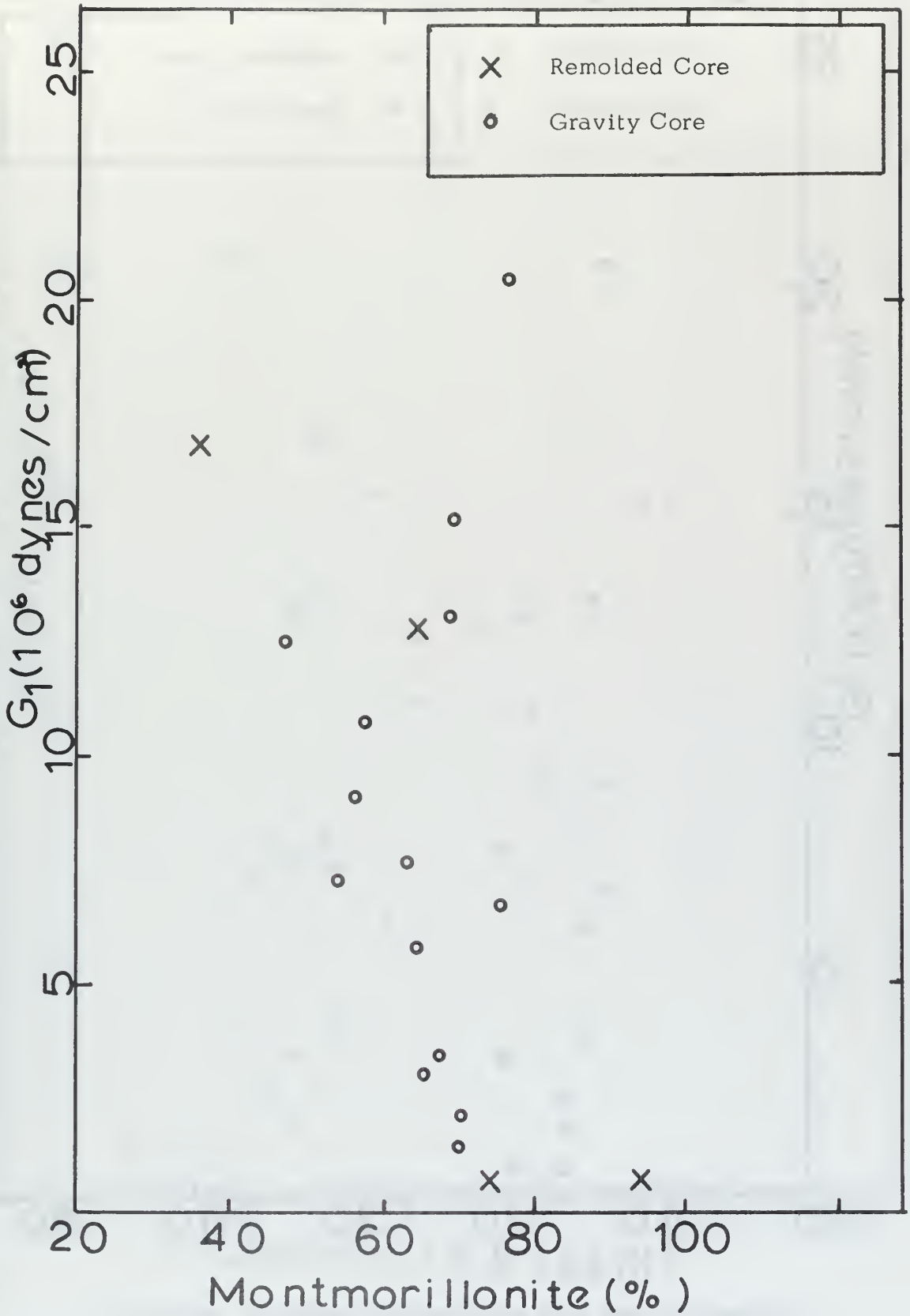

FIGURE 11. G_1 AS A FUNCTION OF PERCENT MONTMORILLONITE.

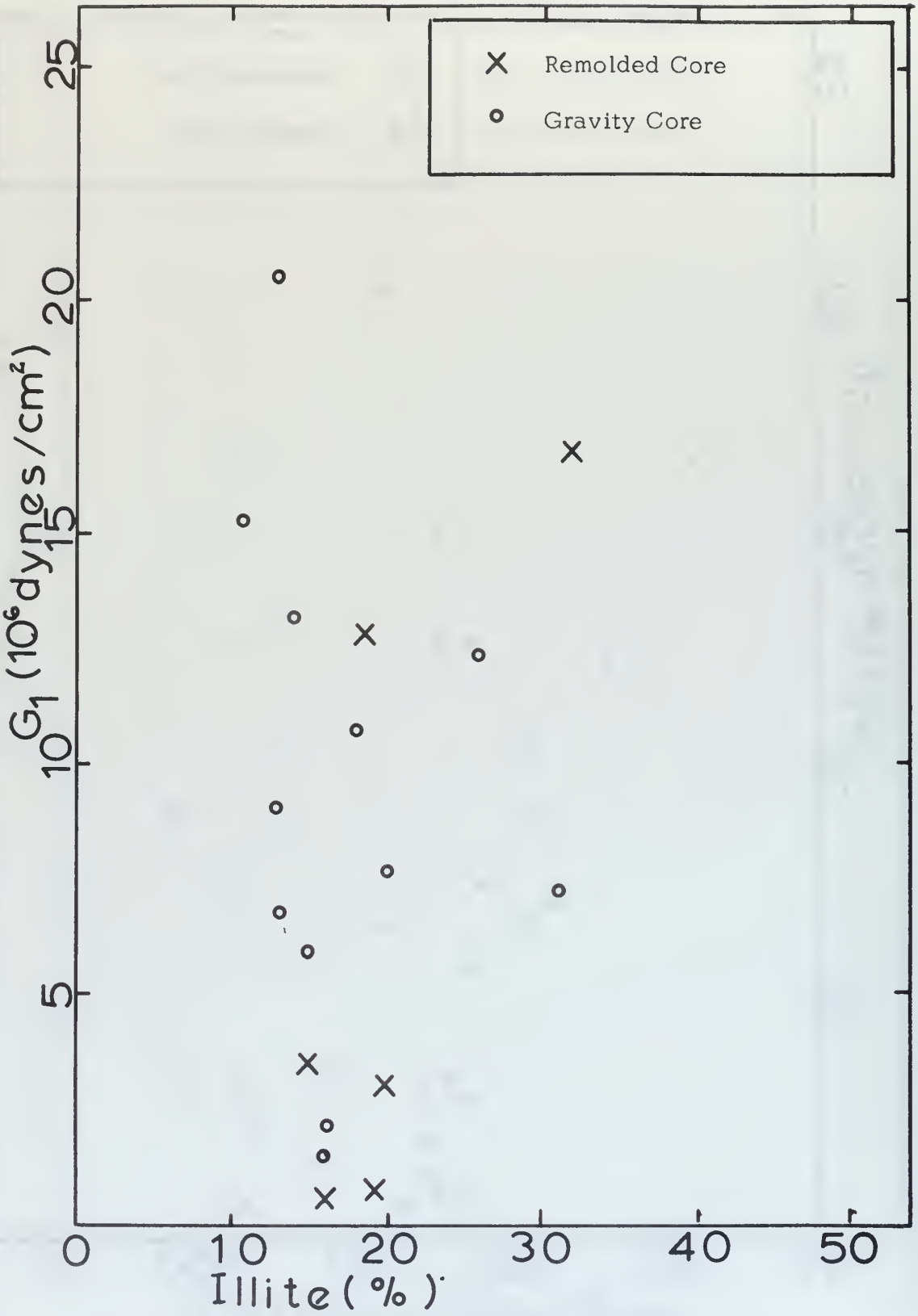

FIGURE 12. G_1 AS A FUNCTION OF PERCENT ILLITE.

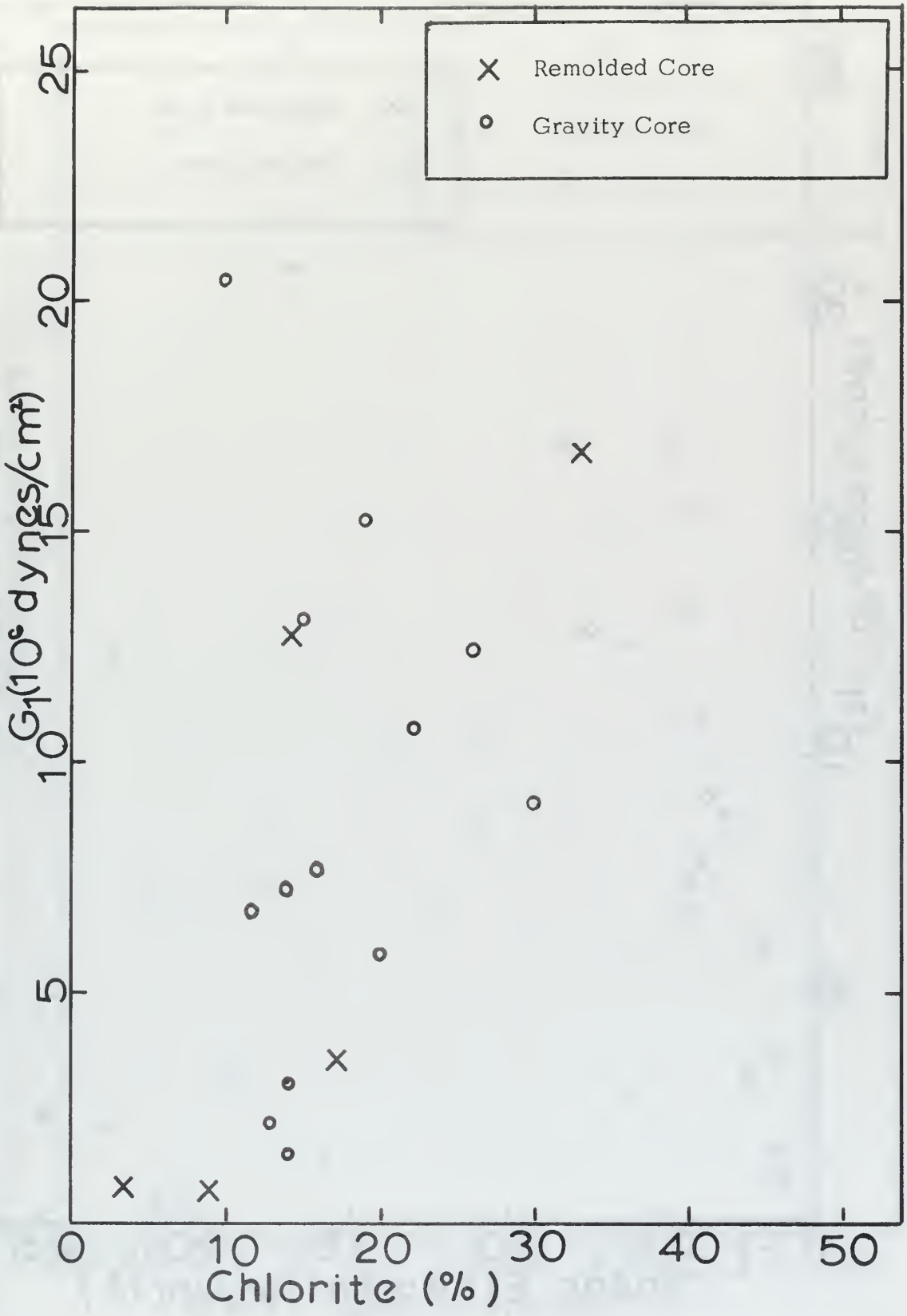

FIGURE 13. G_1 AS A FUNCTION OF PERCENT CHLORITE.

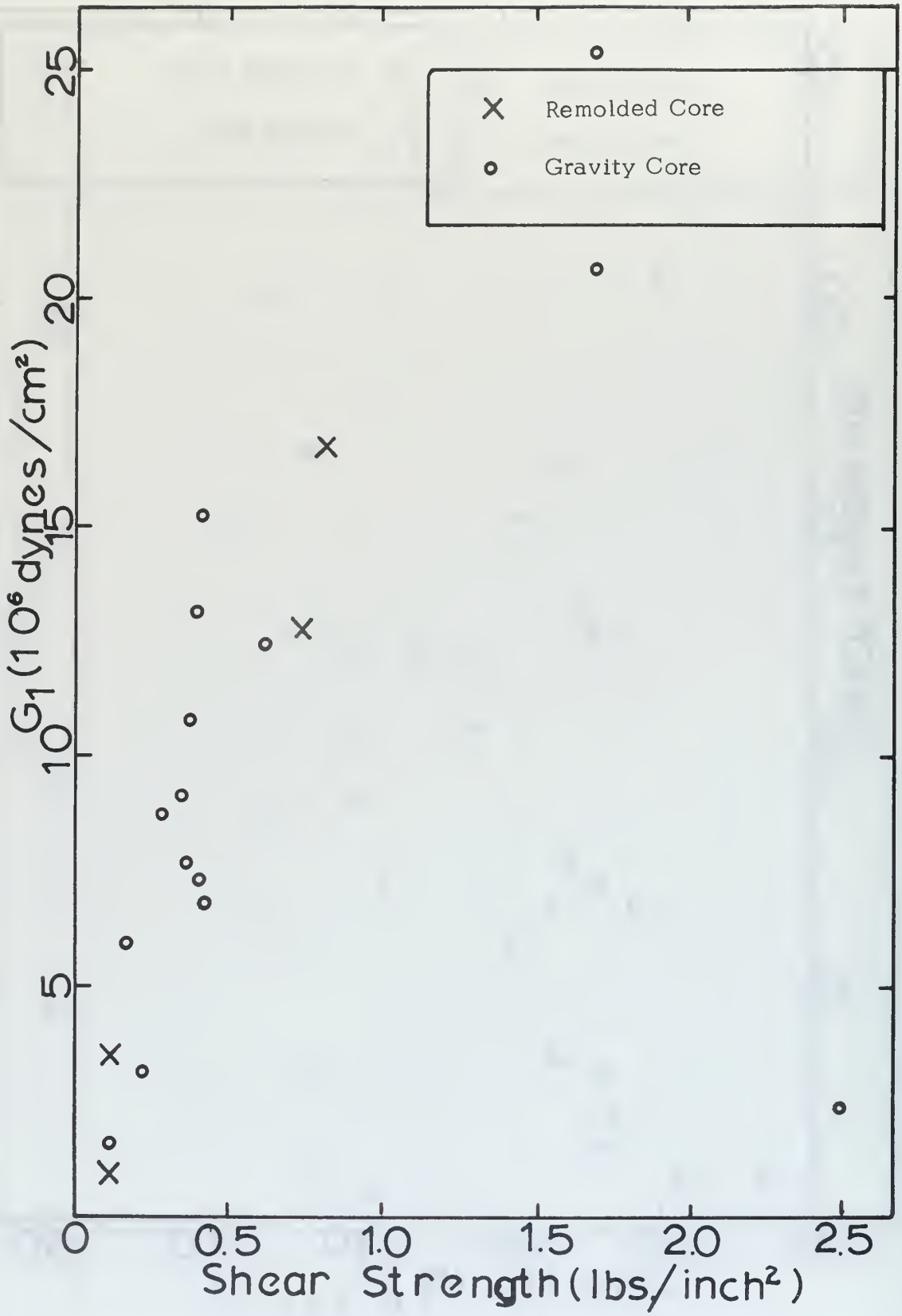

FIGURE 14. G_1 AS A FUNCTION OF VANE SHEAR STRENGTH.

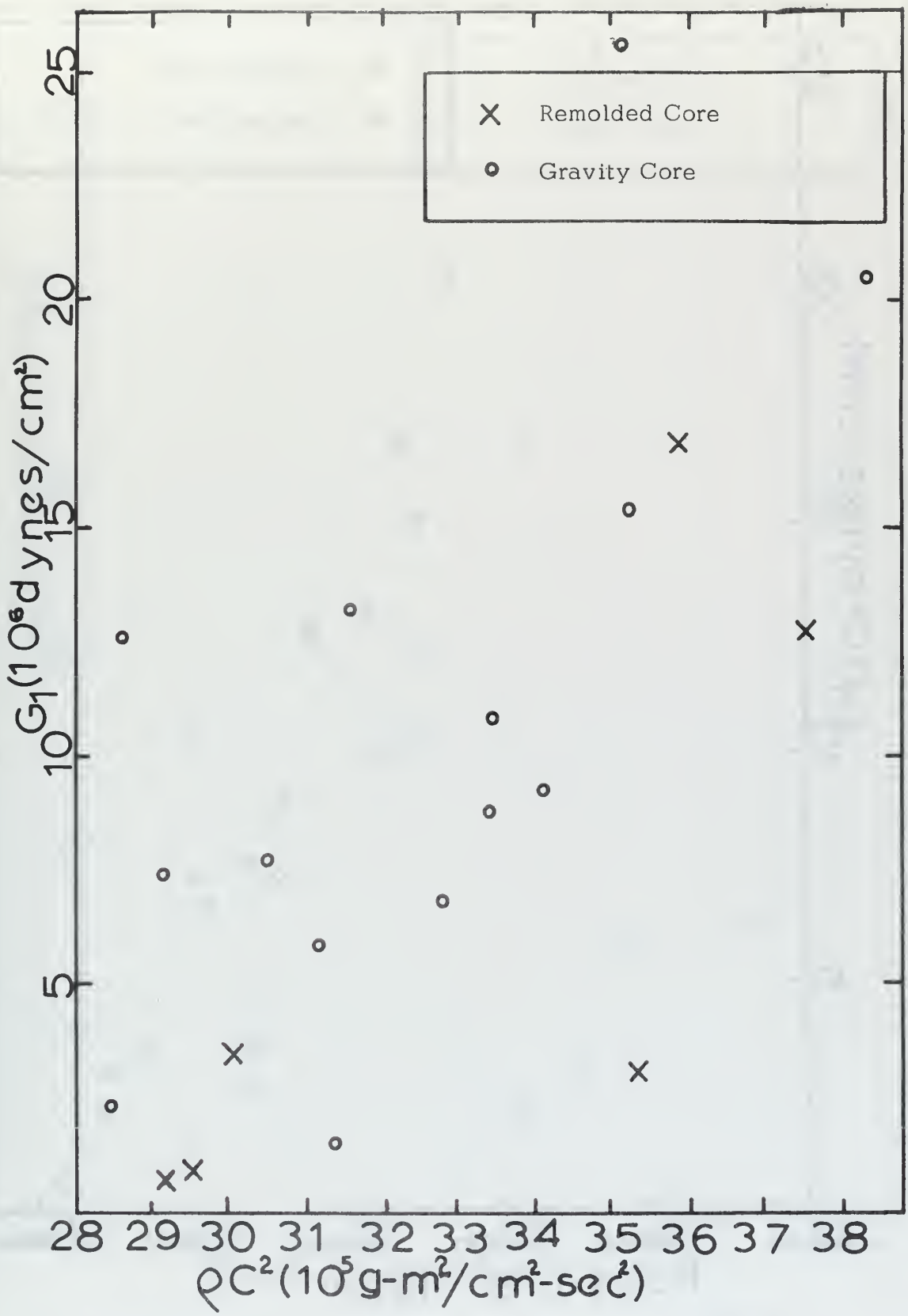

FIGURE 15. G_1 AS A FUNCTION OF DENSITY AND SOUND SPEED SQUARED.

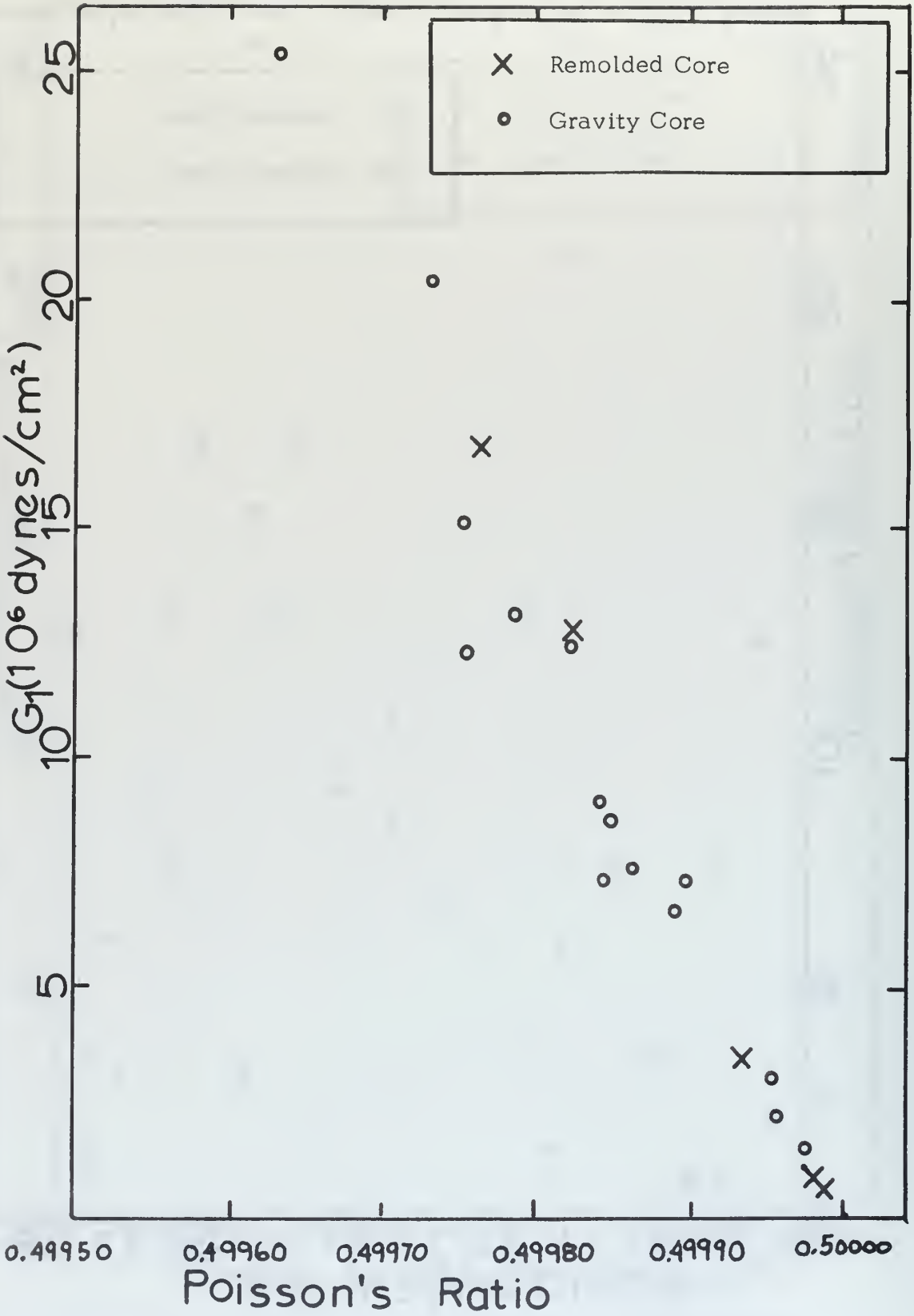

FIGURE 16. G_1 AS A FUNCTION OF POISSON'S RATIO.

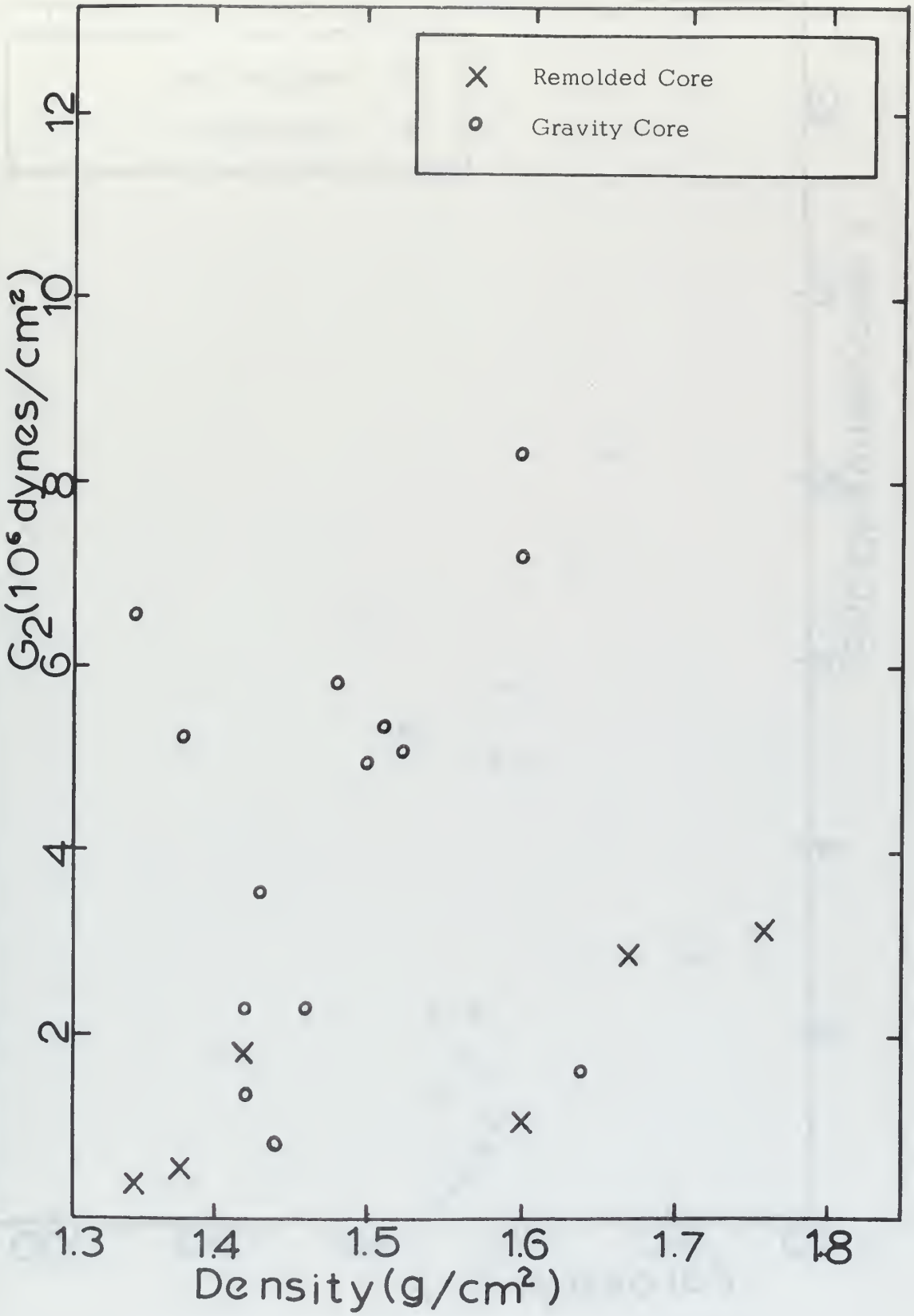

FIGURE 17. G_2 AS A FUNCTION OF DENSITY.

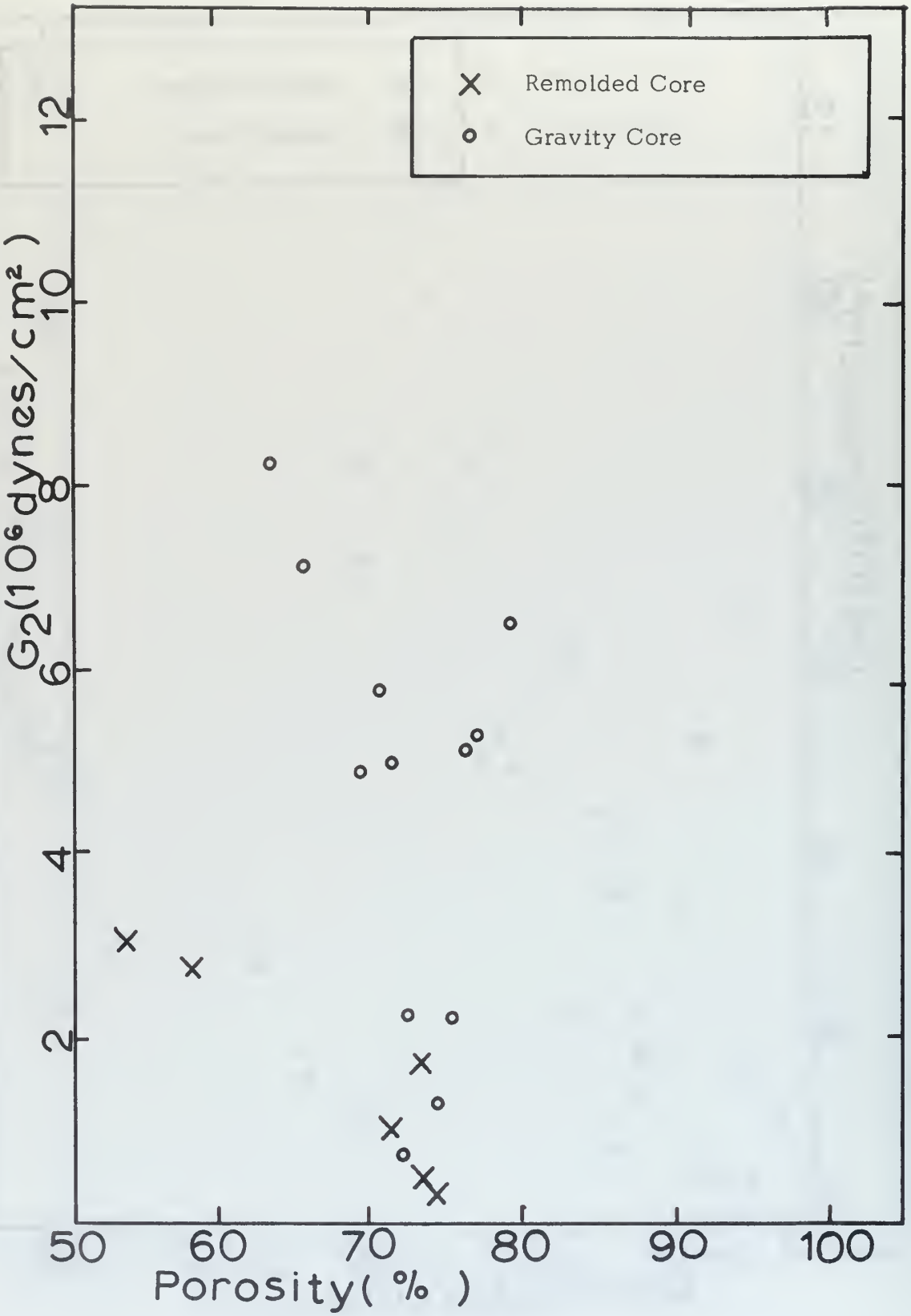

FIGURE 18. G_2 AS A FUNCTION OF POROSITY.

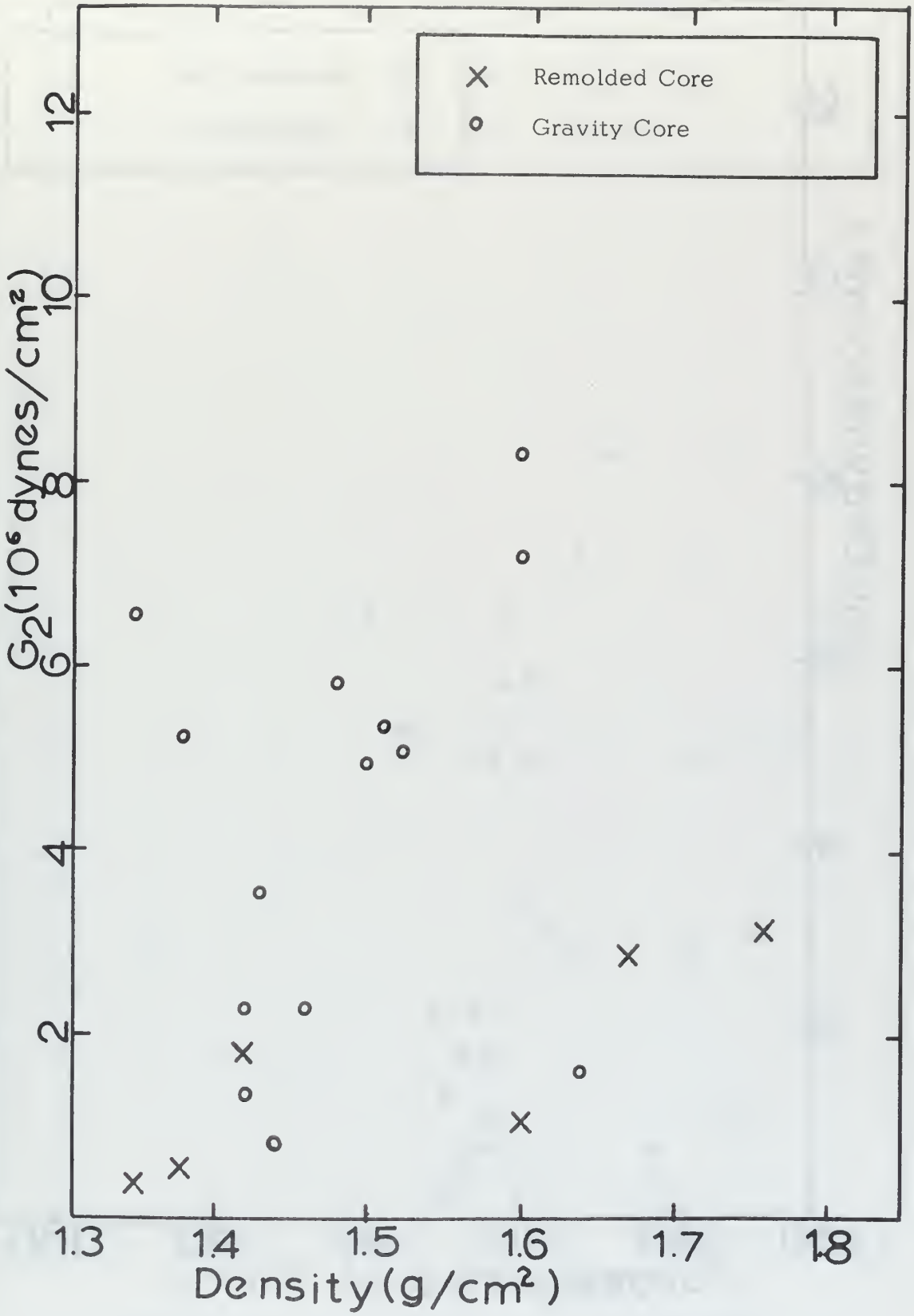

FIGURE 17. G_2 AS A FUNCTION OF DENSITY.

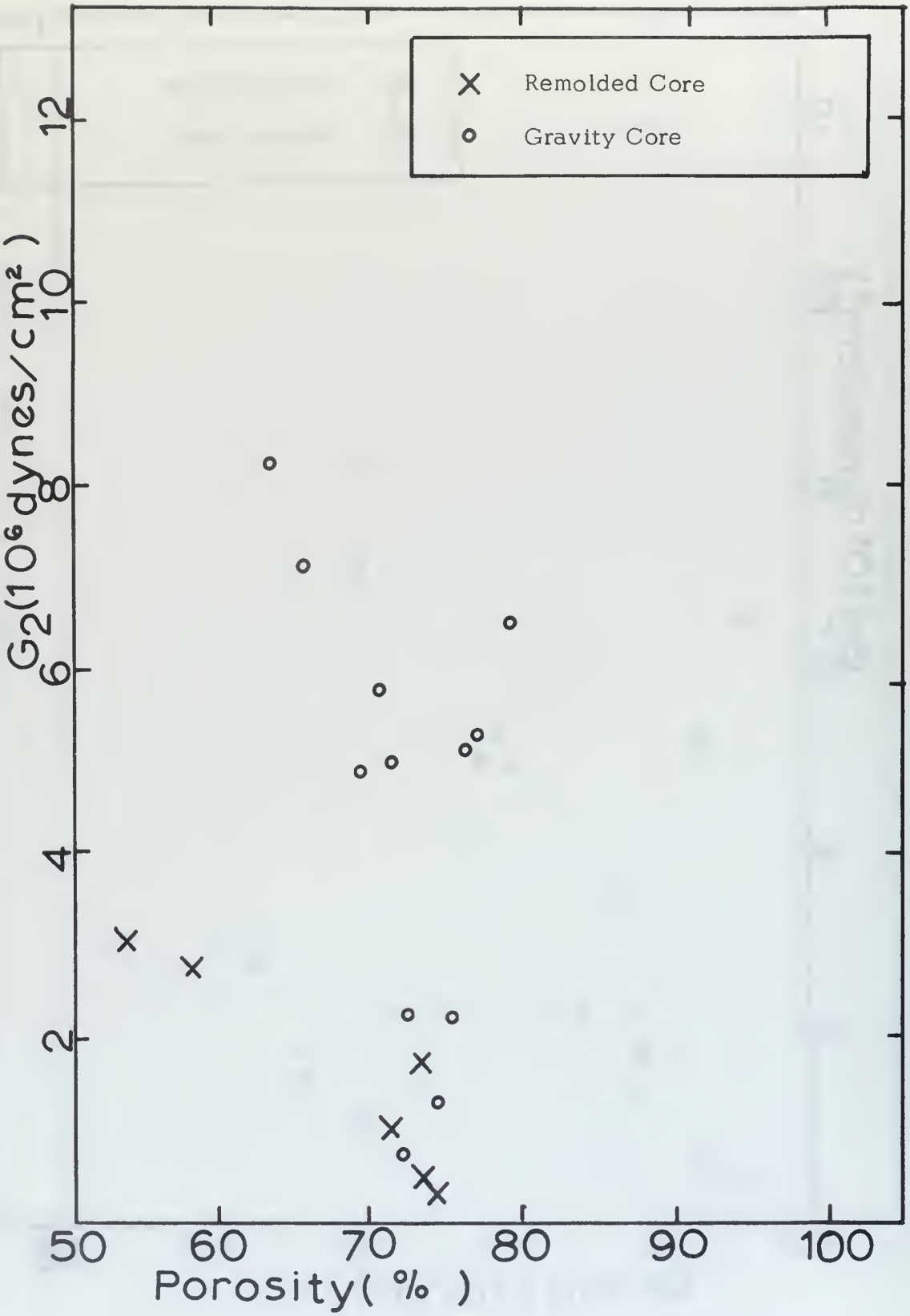

FIGURE 18. G_2 AS A FUNCTION OF POROSITY.

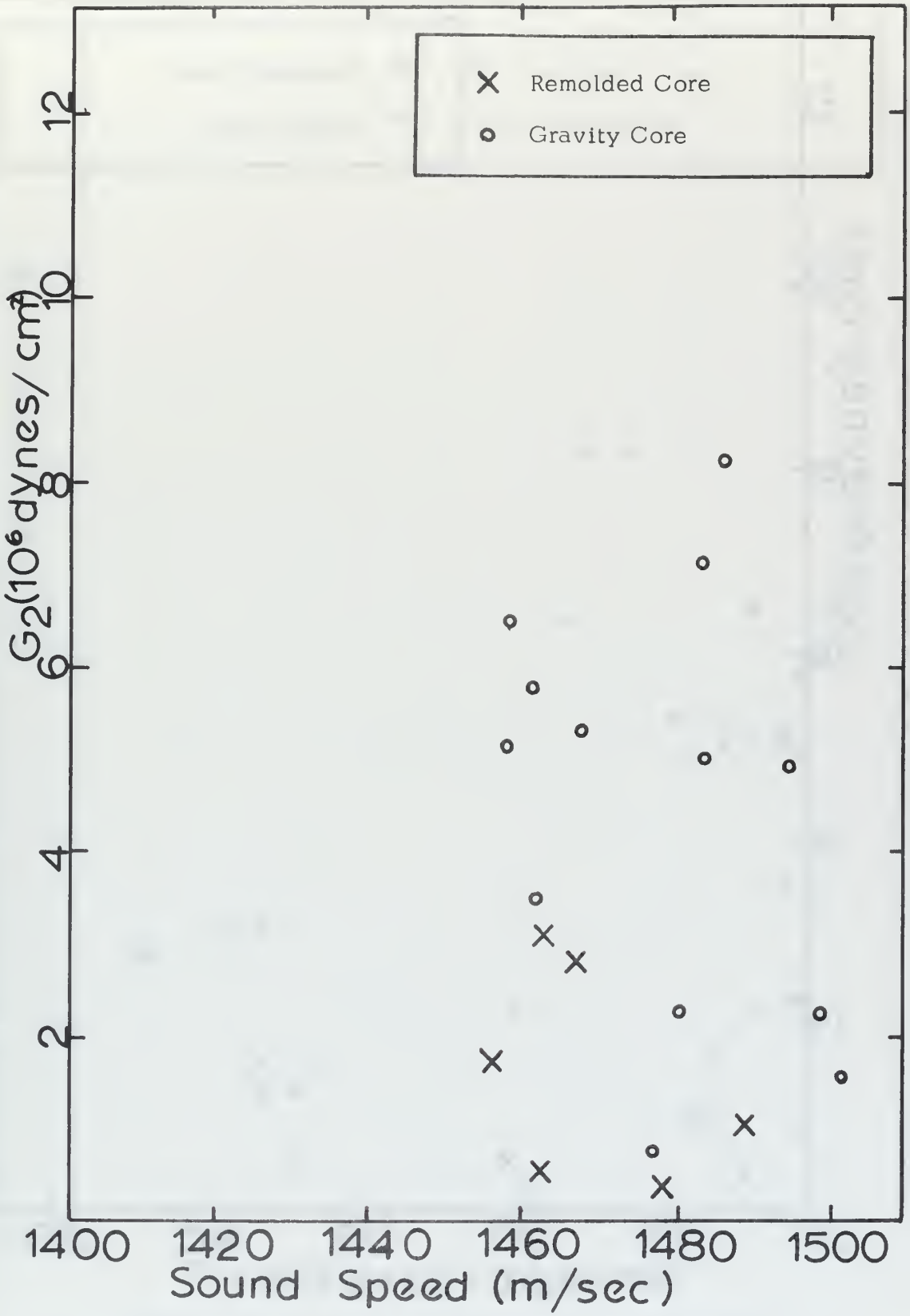

FIGURE 19. G_2 AS A FUNCTION OF SOUND SPEED.

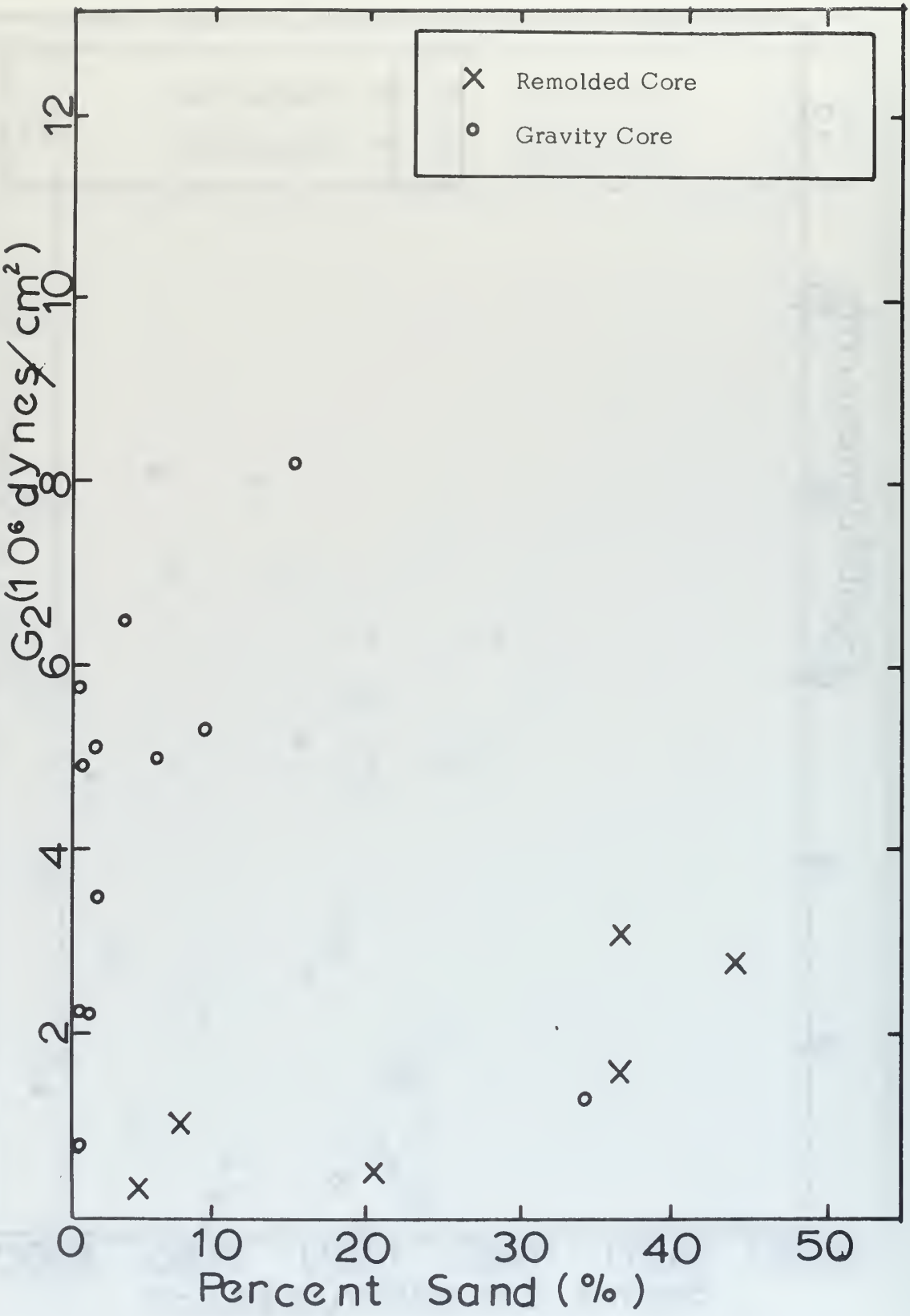

FIGURE 20. G_2 AS A FUNCTION OF PERCENT SAND.

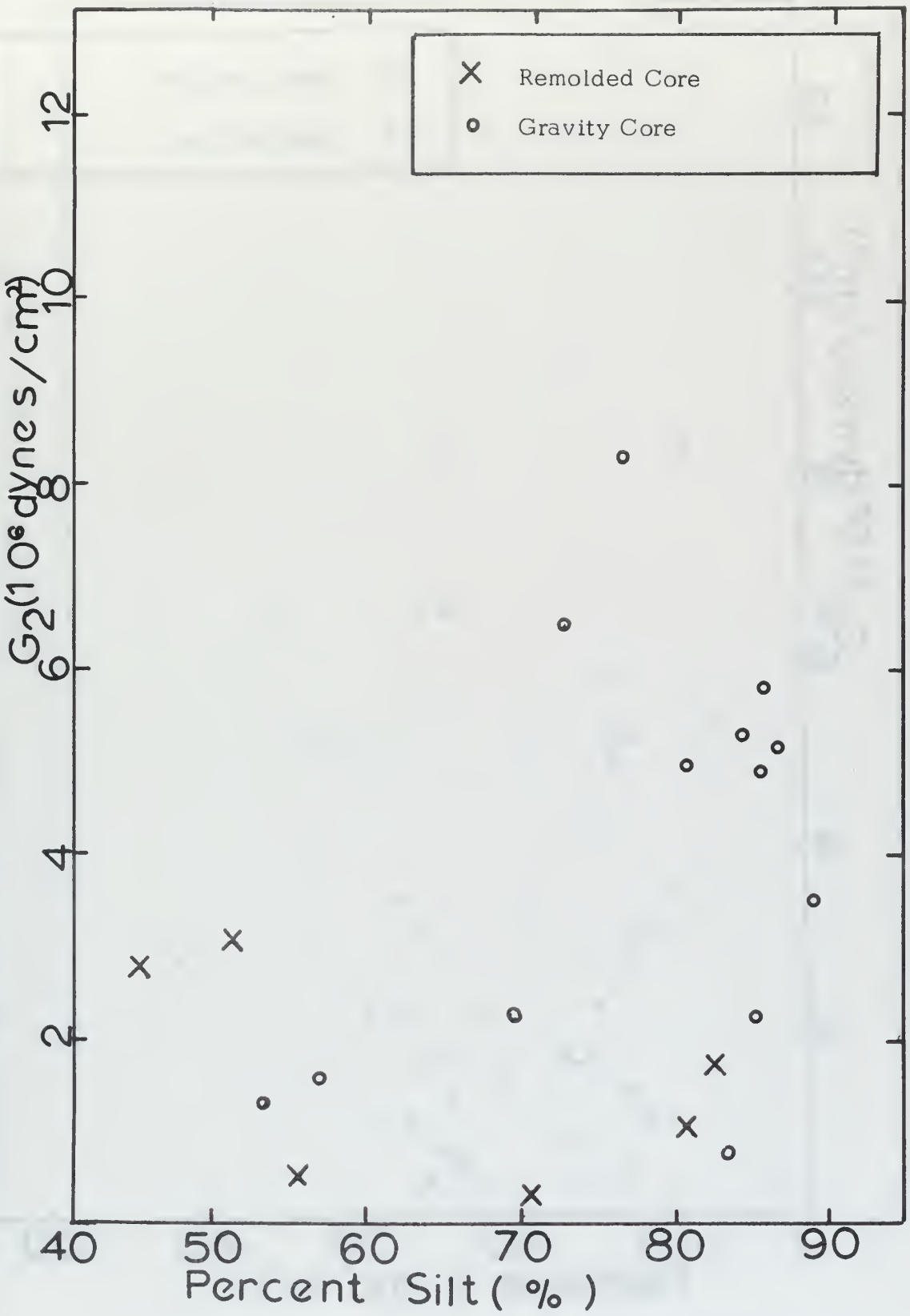

FIGURE 21. G_2 AS A FUNCTION OF PERCENT SILT.

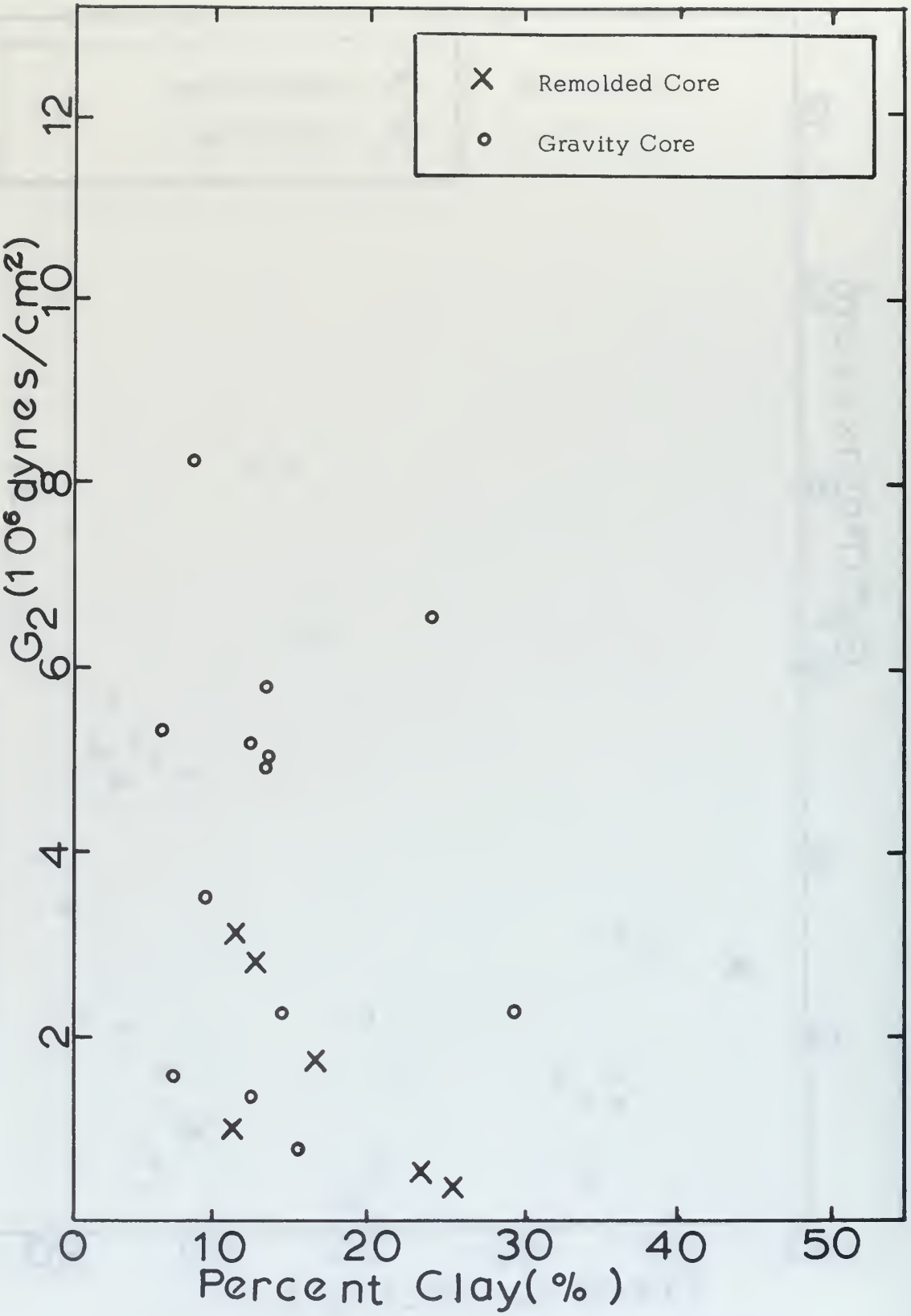

FIGURE 22. G_2 AS A FUNCTION OF PERCENT CLAY.

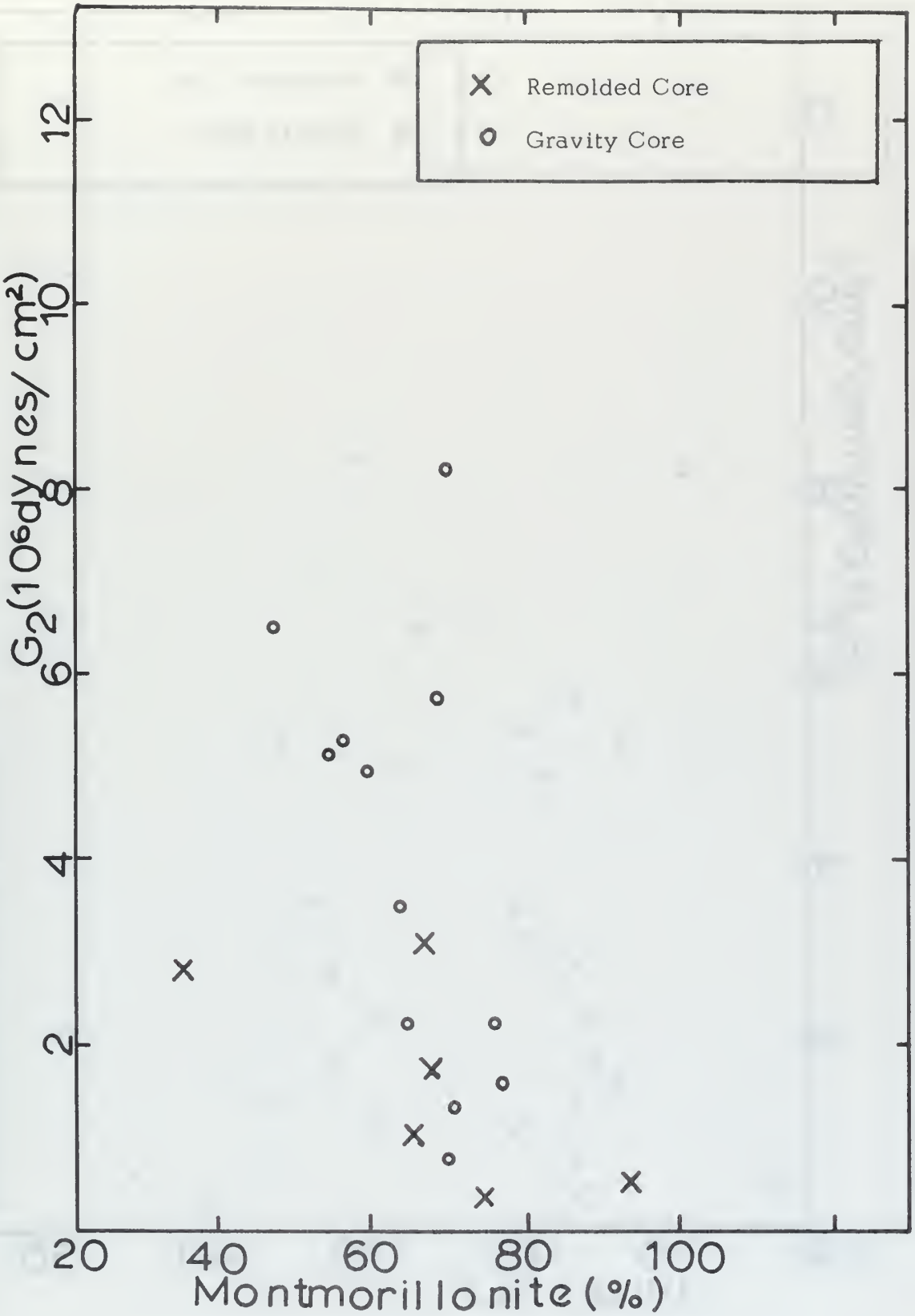

FIGURE 23. G_2 AS A FUNCTION OF PERCENT MONTMORILLONITE.

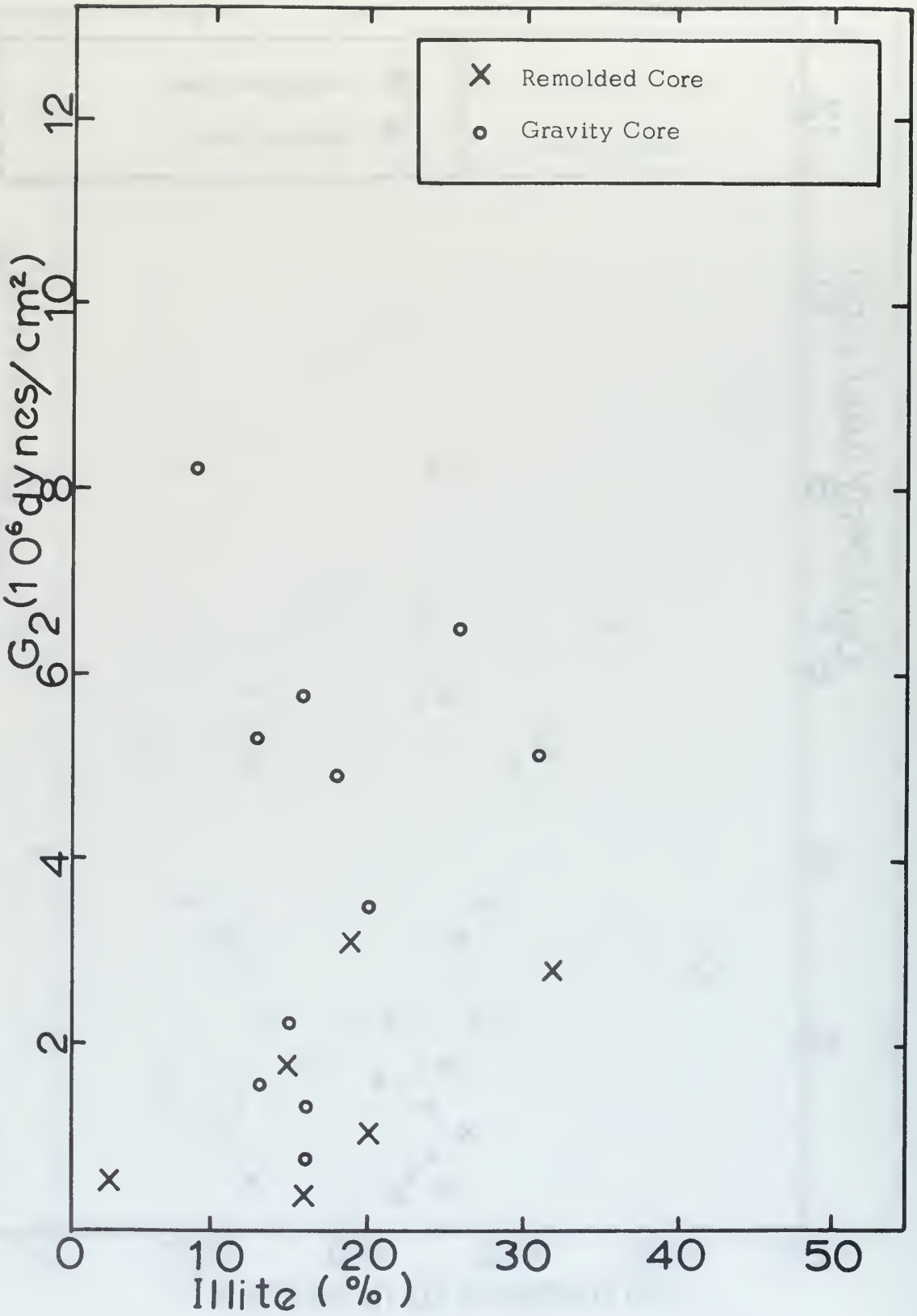

FIGURE 24. G_2 AS A FUNCTION OF PERCENT ILLITE.

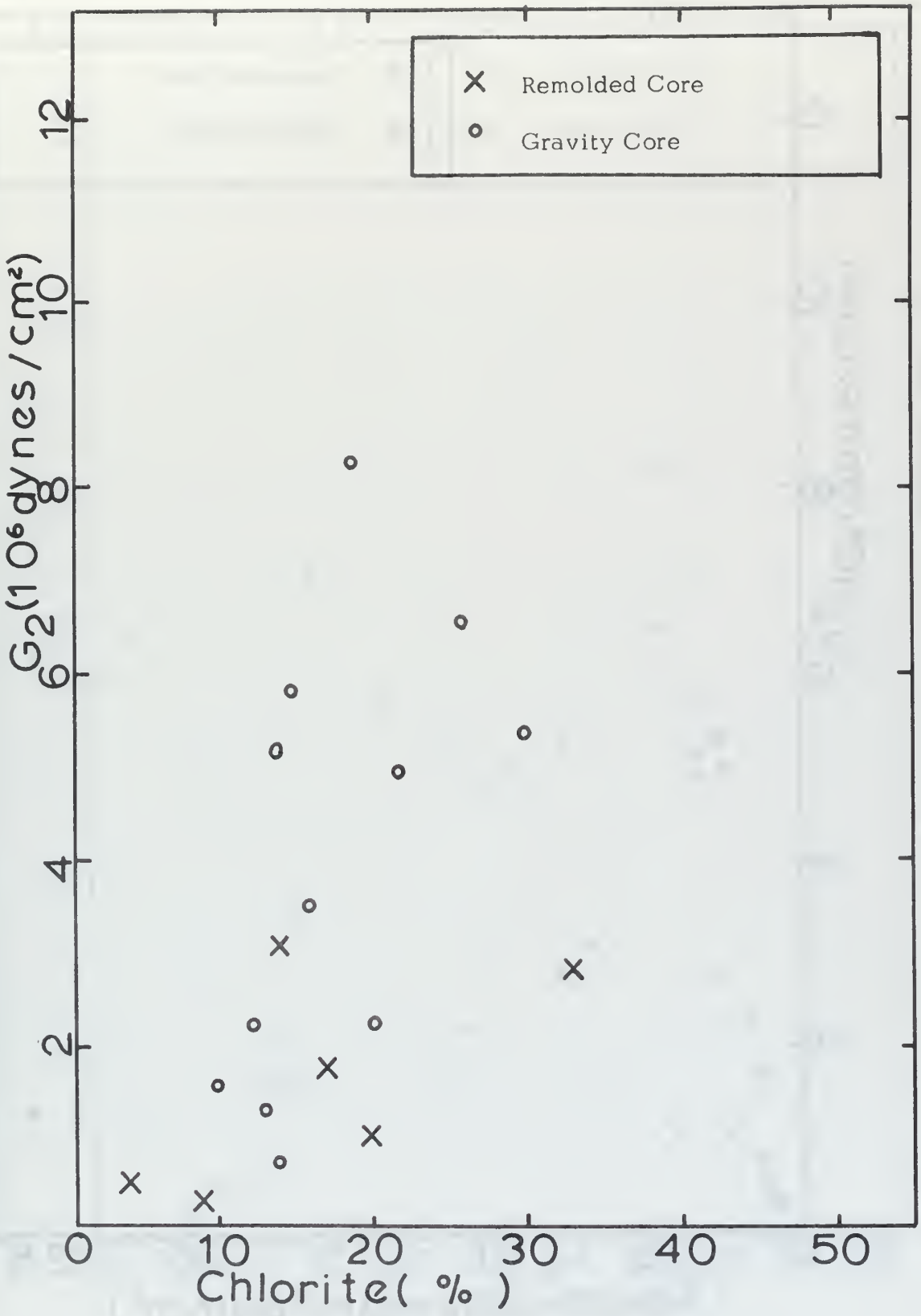

FIGURE 25. G_2 AS A FUNCTION OF PERCENT CHLORITE.

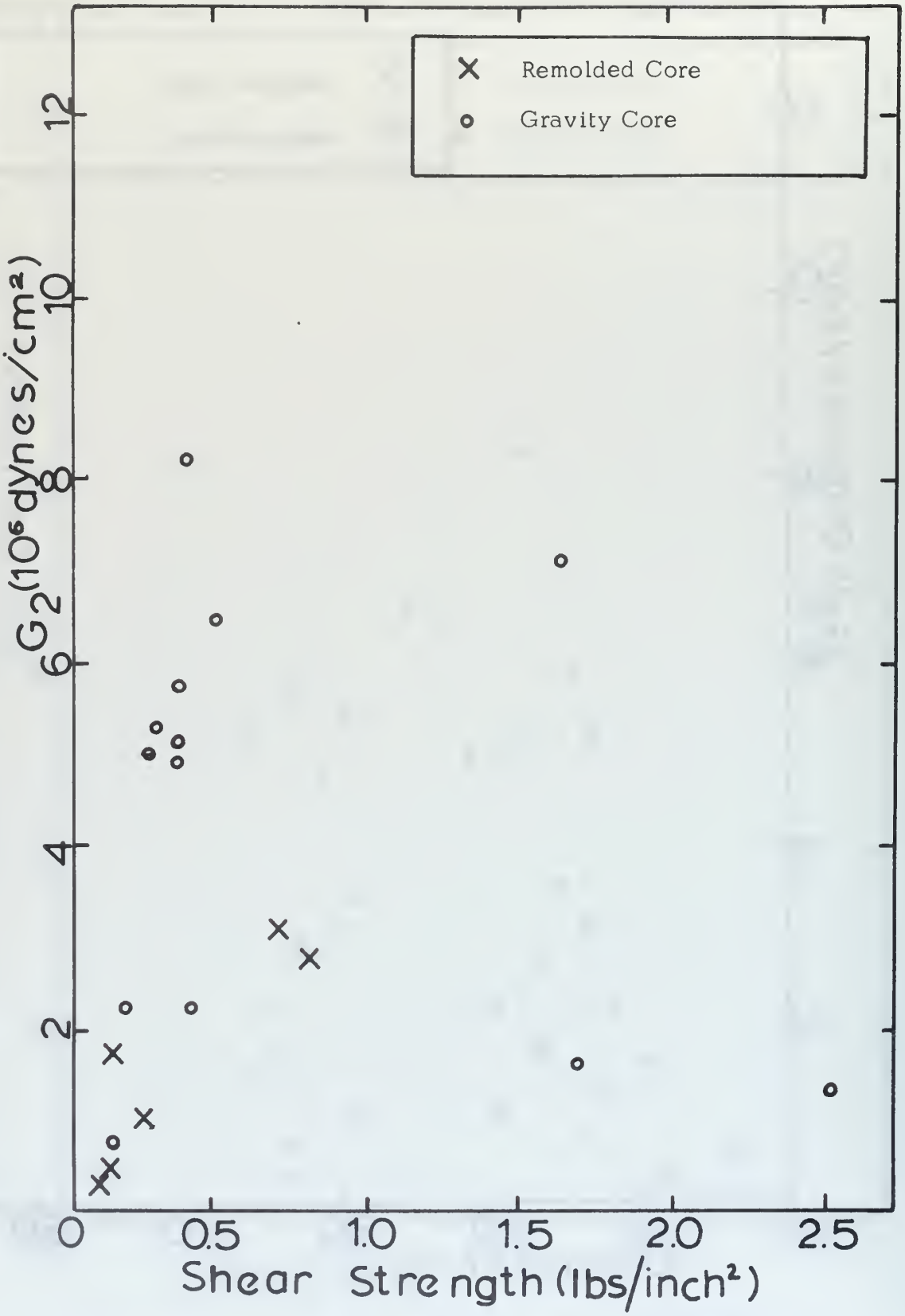

FIGURE 26. G_2 AS A FUNCTION OF VANE SHEAR STRENGTH.

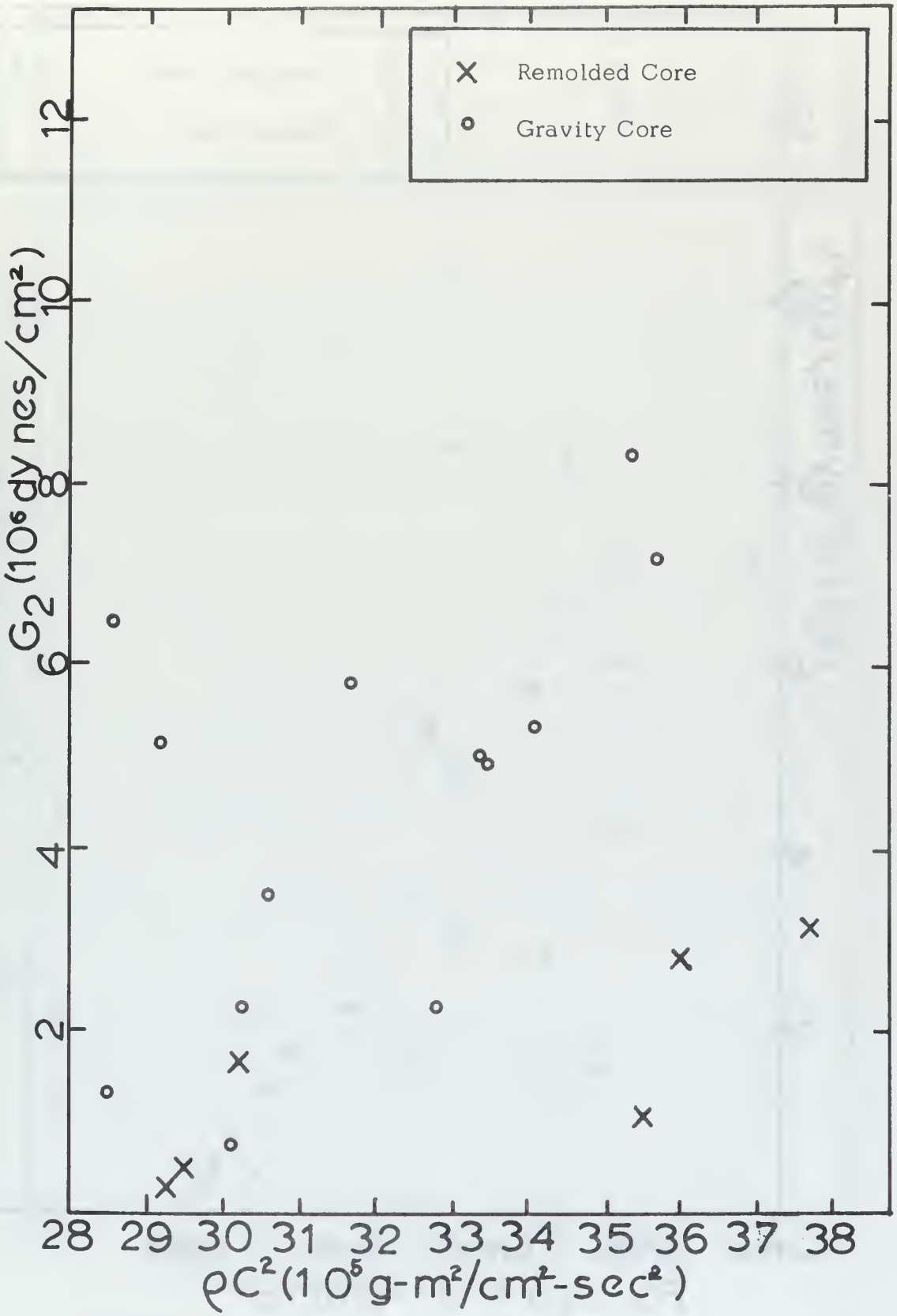

FIGURE 27. G_2 AS A FUNCTION OF DENSITY AND SOUND SPEED SQUARED.

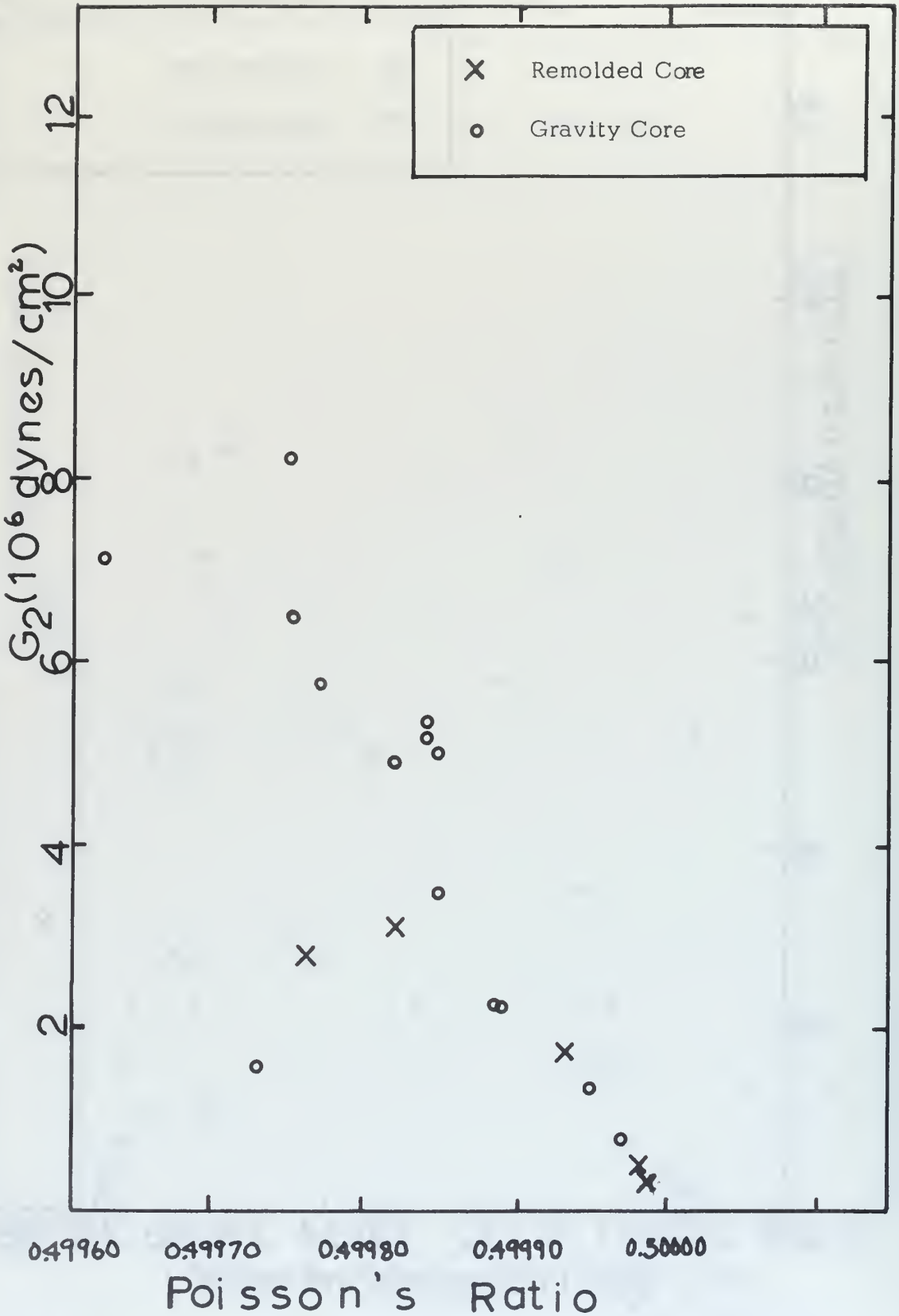

FIGURE 28. G_2 AS A FUNCTION OF POISSON'S RATIO.

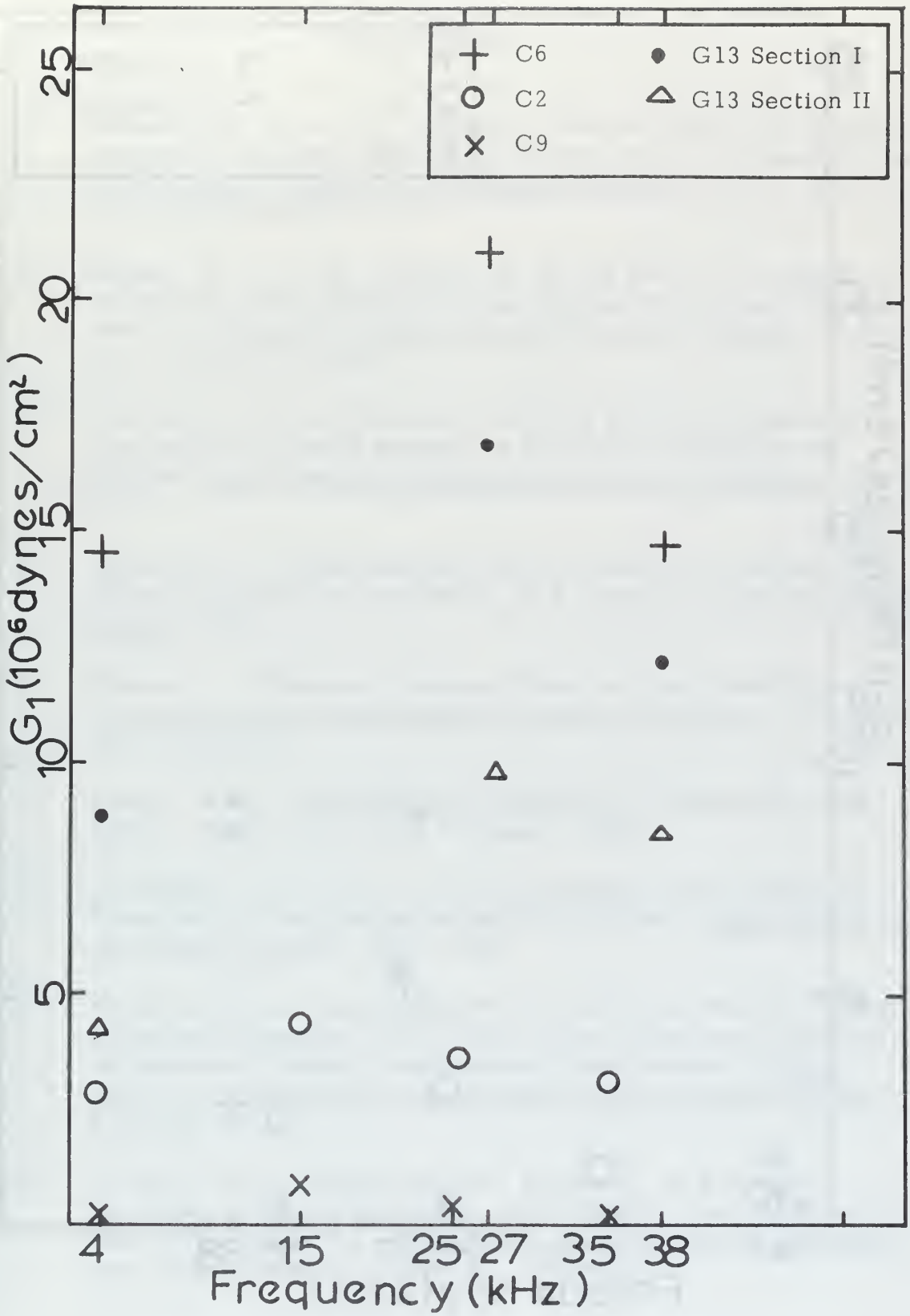

FIGURE 29. G_1 AS A FUNCTION OF FREQUENCY.

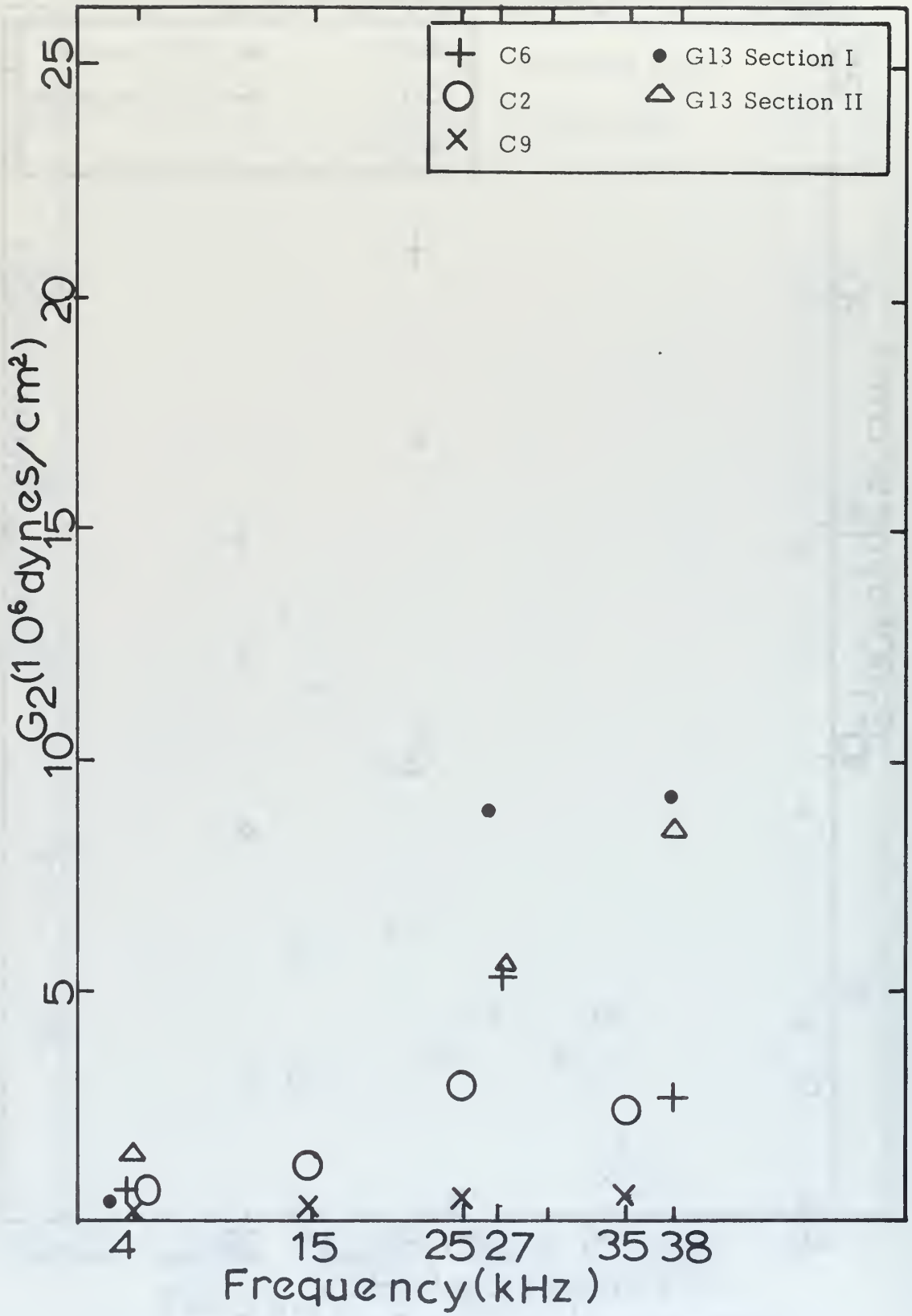

FIGURE 30. G_2 AS A FUNCTION OF FREQUENCY.

BIBLIOGRAPHY

(1) Anderson, R. S. and G. V. Latham, Determination of Sediment Properties from First Shear Mode Rayleigh Waves Recorded on the Ocean Bottom, Journal of Geophysical Research, v. 74, no. 10, 1969, 2747-2757.

(2) Bucker, H. P., J. A. Whitney, G. S. Yee and R. R. Gardner, Reflection of Low-Frequency Sonar Signals from a Smooth Ocean Bottom, The Journal of the Acoustical Society of America, v. 37, no. 6, 1965, 1037-1051.

(3) Cadling, L. and S. Odenstad, The Vane Borer: An Apparatus for Determining the Shear Strength of Clay Soils Directly in the Ground, Royal Swedish Geotechnical Institute Proceedings, no. 2, 1950.

(4) Cohen, S. R., Measurement of the Viscoelastic Properties of Water Saturated Clay Sediments, M.S. Thesis, Naval Postgraduate School, 1968.

(5) Davies, D., Dispersed Stoneley Waves on the Ocean Bottom, The Bulletin of the Seismological Society of America, v. 55, no. 5 1965, 903-918.

(6) Dobrin, M. B., Introduction to Geophysical Prospecting, 2nd Edition, McGraw-Hill Book Company, 1960.

(7) Gallagher, J. J. and V. A. Nacci, Investigations of Sediment Properties in Sonar Bottom Reflectivity Studies, Underwater Sound Laboratory Report No. 944, 1968.

(8) Hamilton, E. L., Sound Velocity, Elasticity and Related Properties of Marine Sediments, North Pacific, Part I: Sediment Properties, Environmental Control, and Empirical Relationships, Naval Undersea Research and Development Center Technical Report No. 143, 1969.

(9) Hamilton, E. L., Sound Velocity, Elasticity and Related Properties of Marine Sediments, North Pacific, Part II: Elasticity and Elastic Constants, Naval Undersea Research and Development Center Technical Report No. 144, 1969.

(10) Hamilton, E. L., H. P. Bucker, D. L. Keir and J. A. Whitney, In Situ Determinations of the Velocities of Compressional and Shear Waves in Marine Sediments from a Research Submersible, Naval Undersea Research and Development Center Technical Report No. 163, 1969.

(11) Hutchins, J. R., Investigation of the Viscoelastic Properties of a Water Saturated Sediment, M.S. Thesis, Naval Postgraduate School, 1967.

(12) Kinsler, L. E. and A. R. Frey, Fundamentals of Acoustics, 2nd Edition, Wiley and Sons, Inc., 1962.

(13) Mason, W. P., Measurements of the Viscosity and Shear Elasticity of Liquids by Means of a Torsionally Vibrating Crystal, Transactions of the A. S. M. E., May 1947, 359-370.

(14) Mason, W. P., Physical Acoustics, v. 2, part B, Academic Press, 1965.

(15) McSkimin, H. J., Measurements of Dynamic Shear Viscosity and Stiffness of Viscous Liquids by Means of Traveling Torsional Waves, The Journal of the Acoustical Society of America, v. 24, no. 4, 1952, 355-365.

(16) Morris, H. E., A Study of the Effect of Sediment Shear Waves on Bottom Reflection Losses in Underwater Acoustics, Naval Undersea Warfare Center Technical Note, No. 7, 1967.

(17) Williard, G. W., Temperature Coefficient of Ultrasonic Velocity in Solutions, The Journal of the Acoustical Society of America, v. 19, no. 1, 1947, 235-241.

INITIAL DISTRIBUTION LIST

		No. Copies
1.	Defense Documentation Center Cameron Station Alexandria, Virginia 22314	2
2.	Library Naval Postgraduate School Monterey, California 93940	2
3.	Dr. O. B. Wilson, Jr. Department of Physics Naval Postgraduate School Monterey, California 93940	10
4.	Dr. R. S. Andrews Department of Oceanography Code 58Ad Naval Postgraduate School Monterey, California 93940	10
5.	Dr. R. Smith Department of Oceanography Naval Postgraduate School Monterey, California 93940	1
6.	Dr. E. L. Hamilton Naval Undersea Warfare Center San Diego, California 92152	1
7.	Dr. G. Griggs Division of Natural Sciences University of California Santa Cruz, California 95060	1
8.	Dr. William R. Bryant Texas A&M University Department of Oceanography College Station, Texas 77843	1
9.	Dr. Davis A. Fahlquist Texas A&M University Department of Geophysics College Station, Texas 77843	1

10.	Dr. P. Cernock c/o R. S. Andrews Code 58Ad Department of Oceanography Naval Postgraduate School Monterey, California	1
11.	Dr. Frederick Bowles Naval Oceanographic Office Washington, D. C. 20390	1
12.	Mr. James J. Gallagher Oceanography Branch Ocean Sciences Division Naval Underwater Sound Laboratory New London, Conn. 06320	1
13.	Mr. H. P. Bucker Naval Research Laboratory Washington, D. C. 20390	1
14.	Mr. Dave Kier Sound Propagation Branch Naval Undersea Research and Development Center San Diego, California 92132	1
15.	Mr. R. S. Anderson Naval Research Laboratory Washington, D. C. 20390	1
16.	LTJG George E. Bieda, USN c/o Edward G. Bieda Box 130A Rt #1 Wapwallopen, Pennsylvania 18660	1
17.	Department of Oceanography Code 58 Naval Postgraduate School Monterey, California 93940	3

DOCUMENT CONTROL DATA - R & D

(Security classification of title, body of abstract and indexing annotation must be entered when the overall report is classified)

1. ORIGINATING ACTIVITY *(Corporate author)*

Naval Postgraduate School
Monterey, California 93940

2a. REPORT SECURITY CLASSIFICATION

2b. GROUP

3 REPORT TITLE

4 DESCRIPTIVE NOTES *(Type of report and, inclusive dates)*

Master's Thesis; June 1970

5. AUTHOR(S) *(First name, middle initial, last name)*

George E. Bieda

6. REPORT DATE: June 1970

7a. TOTAL NO. OF PAGES: 75

7b. NO. OF REFS: 17

8a. CONTRACT OR GRANT NO.

b. PROJECT NO.

c.

d.

9a. ORIGINATOR'S REPORT NUMBER(S)

9b. OTHER REPORT NO(S) *(Any other numbers that may be assigned this report)*

10 DISTRIBUTION STATEMENT

This document has been approved for public release and sale; its distribution is unlimited.

11. SUPPLEMENTARY NOTES

12. SPONSORING MILITARY ACTIVITY

Naval Postgraduate School
Monterey, California 93940

13. ABSTRACT

The complex rigidity of 20 samples of continental terrace clayey-silt sediments has been measured in the laboratory using a viscoelastometer in the frequency range from 4 to 38 kHz. The method involves measuring the effects on torsional waves propagating in a rod due to shear loading of the side walls of the rod when it is imbedded in the sediment. Values of the real component of rigidity range from 6.5×10^5 to 2.6×10^7 dynes/cm^2. Values of the imaginary component of rigidity fall between 2.9×10^5 and 8.2×10^6 dynes/cm^2. No clear-cut dependence of rigidity upon frequency is observed. Both real and imaginary components of rigidity are analyzed by plotting the data as a function of various other mass-physical properties, including: density, porosity, compressional sound speed, sand-silt-clay percentages, montmorillonite, chlorite, illite percentages, vane shear strength, Poisson's ratio, and the product of density and sound speed squared. These analyses indicate that both real and imaginary components of rigidity exhibit trends with some of the mass-physical properties.

14 KEY WORDS	LINK A		LINK B		LINK C	
	ROLE	WT	ROLE	WT	ROLE	WT
Viscoelastic						
Shear Modulus						
Rigidity						
Sediment						

Thesis
B512 Bieda
c.1 Measurement of the visco elastic and related mass-physical properties of some continental terrace sediments.
120743

Thesis
B512 Bieda
c.1 Measurement of the visco elastic and related mass-physical properties of some continental terrace sediments.
120743

thesB512
Measurement of the visco elastic and rel
3 2768 002 13438 9
DUDLEY KNOX LIBRARY